

# Ultramafic xenoliths from the Veneto Volcanic Province (Italy): Petrological and geochemical evidence for multiple metasomatism of the SE Alps mantle lithosphere

DANIELA GASPERINI,<sup>1</sup> DELPHINE BOSCH,<sup>2</sup> ROBERTO BRAGA,<sup>3</sup> MIRELLA BONDI,<sup>3</sup>  
PATRIZIA MACERA<sup>1\*</sup> and LAURO MORTEN<sup>3</sup>

<sup>1</sup>Dipartimento di Scienze della Terra, Università di Pisa, via S. Maria 53, 56126 Pisa, Italy

<sup>2</sup>Laboratoire Tectonophysique, Université Montpellier 2, UMR-CNRS 5568, 22 Place Bataillon, 34095 Montpellier, France

<sup>3</sup>Dipartimento Scienze della Terra e Geologico Ambientali, Università di Bologna, Piazza Porta S. Donato 1, Bologna, Italy

(Received June 2, 2005; Accepted January 24, 2006)

Ultramafic (mg# > 88) xenoliths from the Tertiary Veneto Volcanic Province (SE Alps, Italy) are characterized by variable depletion due to removal of a basaltic component and show significant trace element and isotopic (<sup>87</sup>Sr/<sup>86</sup>Sr: 0.703031–0.704356; <sup>143</sup>Nd/<sup>144</sup>Nd: 0.512817–0.513085; <sup>206</sup>Pb/<sup>204</sup>Pb: 18.539–19.694; <sup>207</sup>Pb/<sup>204</sup>Pb: 15.608–15.658; <sup>208</sup>Pb/<sup>204</sup>Pb: 38.412–39.660; δ<sup>18</sup>O: 6.6–11.2‰) heterogeneity. Variable large-ion lithophile and light rare earth/high field strength element ratios and isotopic compositions occur in samples showing comparable mineralogy and major element content. Petrologic and geochemical characteristics of whole rocks and minerals may be explained by metasomatism of the local mantle lithosphere induced by both alkaline magmas upwelling to the surface (OIB-like mantle diapirism) and interaction with slab-derived material. In comparison with the geochemistry of xenoliths carried by alkaline magmas in typical within-plate tectonic environments, the Veneto xenoliths record a major heterogeneity of the local lithosphere. This appears to be related to a geodynamic scenario that was previously dominated by active continental collision, in which plume-like magmatism subsequently manifested itself.

Keywords: mantle xenoliths, petrology, geochemistry, north-eastern Italy, heterogeneous lithosphere

## INTRODUCTION

The upper mantle cannot be investigated by direct sampling, so peridotite xenoliths hosted in basaltic rocks provide a useful way to define its characteristics, such as bulk composition, mineral phase chemistry, occurrence and types of metasomatic processes. Xenoliths from the Veneto Volcanic Province (VVP, SE Alps, NE Italy; Fig. 1) represent the subcontinental lithospheric mantle belonging to the African plate beneath the Veneto region. They are hosted by sodic-alkaline extension-related magmas (Macera *et al.*, 2003). During the Cretaceous, the surrounding SE Alps were involved in convergence between Africa and Eurasia plates, inducing subduction processes of the latter plate southeastward (von Blanckenburg and Davies, 1995; Schmid *et al.*, 1997). Because the subcontinental mantle lacks significant convection, the VVP xenoliths may bear the geochemical and petrographic signature of metasomatism induced by di-

verse geodynamic processes occurring in the Veneto area for the last hundred million years.

Many authors (e.g., Morten, 1971; Morten, 1987; Morten and Bondi, 1981; Siena and Coltorti, 1989; Morten and De Francesco, 1991; Coltorti *et al.*, 2000; Beccaluva *et al.*, 2001; Bonadiman *et al.*, 2001; Morten *et al.*, 2002) have studied mantle xenoliths hosted in alkali basalts and basanites from the Lessini Mts. in the Veneto area (Fig. 1). Petrologic evidence shows that these xenoliths are harzburgites and lherzolites re-equilibrated under spinel-facies conditions (Morten, 1987; Morten and Bondi, 1981). Two series of xenoliths were identified (Morten and Bondi, 1981): the Mg-rich series [mg# = molar MgO/(MgO + FeO<sub>tot</sub>) > 88] and the Fe-rich series (mg# < 88). Both series are depleted in a basaltic component (Morten, 1987). The composition of the most depleted xenoliths is consistent with up to 20% of extracted melt (Morten, 1987; Morten *et al.*, 1989; Hegner *et al.*, 1990). Evidence of melting/metasomatic events, and Ti, Mn and Fe enrichments, are well documented in the form of glass blebs in primary clinopyroxenes, glass veinlets at grain boundaries, glassy patches, and wehrlite portions within the harzburgite-lherzolite xenoliths (Morten, 1987; De Francesco and Morten, 1991; Beccaluva *et al.*, 2001).

\*Corresponding author (e-mail: macera@dst.unipi.it)

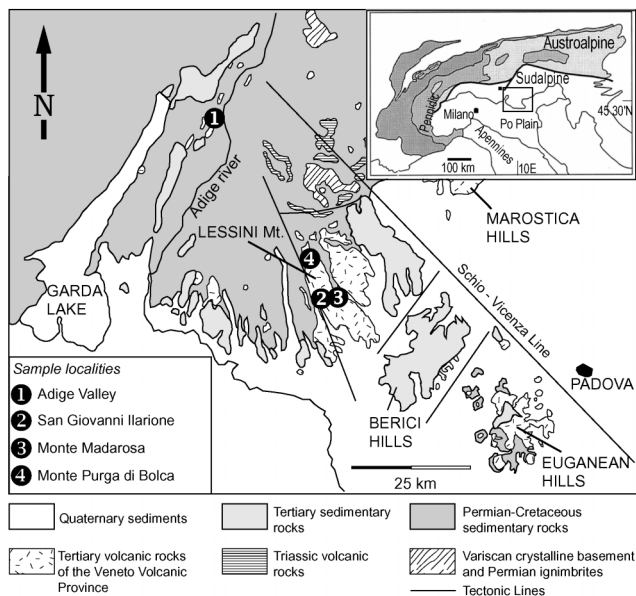


Fig. 1. Sketch map of the south-eastern portion of the southalpine domain (Veneto region) after De Vecchi and Sedeà (1995, modified), and location of the sampled areas.

Beccaluva *et al.* (2001) suggested that the addition of 1–6% of a Na-alkaline melt to a primary lherzolite composition may account for the present petrologic and geochemical composition of a typical lherzolite. Nevertheless, the occurrence of ultrapotassic, benmoreitic and other glass compositions suggests that different metasomatic agents and processes occurred.

In this work we describe petrologic, geochemical and isotopic (Sr, Nd, Pb and O) features of a new suite of Mg-rich (i.e. mg# > 88) spinel peridotite xenoliths from different outcrops of the Adige Valley and Lessini Mts. (Fig. 1). This study focuses on fresh whole-rock samples to investigate processes of melting and metasomatism that likely gave rise to the compositional heterogeneity recorded in the lithospheric mantle beneath the Veneto region. To achieve this goal, the VVP xenoliths are compared to representative worldwide ultramafic xenoliths from different geodynamic settings, such as those carried to the surface by: a) within-plate alkali basalts, in both oceanic (Canary Islands, Kerguelen Islands) and continental environments (French Massif Central, Germany, Australia), b) calc-alkaline magmas in typical subduction zones (Marianas, Papua New Guinea, Philippines) and c) alkali basalts in both extensional and subduction-related geodynamic settings, e.g., along the Pacific plate borders (Russia, China, Mongolia, Japan, Canadian Cordillera), at Vulture (central southern Apennine chain, Italy) and in the Pannonian Basin (Hungary, Romania).

## TECTONO-MAGMATIC OUTLINE

The Veneto Volcanic Province occurs in the eastern-central sector of the south Alpine domain (northeastern Italy; Fig. 1). During the Tertiary, convergence between Africa and Europe induced a south-eastward subduction of the European plate underneath the African plate, giving rise to the Alpine belt, and subsequently to numerous calc-alkaline intrusions and subalkaline dykes of mainly Oligocene age. In the south Alpine eastern foreland (e.g., in the Veneto region), however, an extension-related magmatism of mainly basic composition occurred from late Paleocene to early Miocene times (De Vecchi and Sedeà, 1995; Zampieri, 1995; Milani *et al.*, 1999). According to Maffei *et al.* (2003), the OIB-like alkaline basaltic volcanism in the Veneto region could be related to mantle diapirism. Upwelling of deep mantle material seems to have occurred twice in the south-eastern Alps: first in Paleocene times, i.e. before the subducted European lithospheric slab became an obstacle to deep mantle upwelling, and again during middle Eocene times, through a gap created in the subducting slab by its breakoff (Macera *et al.*, 2003; Ranalli *et al.*, 2004). Veneto volcanics developed over a time span of about 35 Ma, the apex of the volcanic activity occurring in the middle Eocene (De Vecchi and Sedeà, 1995). The most representative rock types are alkali basalts, basanites and transitional basalts, frequently hosting mantle xenoliths.

## SAMPLING AND PETROGRAPHY

Eighteen mantle xenoliths from the Val di Serra quarry (Adige Valley) and twelve xenoliths from Lessini Mts. were used in this study to supplement existing petrographic and geochemical data from the Lessini Mts. (Morten, 1987; Table 1). The locations of the Lessini samples are: San Giovanni Ilarione, Monte Madarosa and Monte Purga di Bolca (Fig. 1). The sampling sites are characterized by several basaltic intrusions represented by 1–2 m thick basaltic dykes (Adige Valley) and tens meters size pipes (Lessini Mts.).

The ultramafic xenoliths are generally sub-rounded, rarely angular. Their size varies from 5 cm to 15 cm in diameter. Generally, the Adige Valley xenoliths invariably show protogranular texture whereas the xenoliths from the Lessini Mts. show more variable textures, from protogranular to porphyroclastic and pyrometamorphic (Pike and Schwarzman, 1977). A significant difference between the Adige Valley xenoliths and those from the Lessini Mts. is that the latter contain glassy patches (Morten and De Francesco, 1991). Hydrous phases, e.g., micas and/or amphiboles, are absent in the Mg-rich series of the VVP xenoliths. The following description gives petrographic details of the selected samples grouped according to their geographical occurrence.

Table 1. Provenance, texture and modal estimates of the studied samples

Sample	Lithotype	Locality	Texture	Modal abundances				
				Ol	Opx	Cpx	Spl	Ol and/or Opx serpentinization
55B	sp-harzburgite	Adige Valley	Protogranular. Intruded by the host	91	7	—	2	+ + +
56B	sp-lherzolite	Adige Valley	Protogranular	65	5	26	4	+
F56-1	sp-lherzolite	Adige Valley	Protogranular	78	12	9	1	+ +
F56-2A	sp-lherzolite	Adige Valley	Protogranular	64	5	27	4	+ + +
F56-2B	sp-lherzolite	Adige Valley	Protogranular	60	33	5	2	+
F56-3	sp-harzburgite	Adige Valley	Protogranular	70	27	1	2	+
F56-4	sp-lherzolite	Adige Valley	Protogranular	75	19	5	1	+ +
F56-5	sp-harzburgite	Adige Valley	Protogranular	83	13	2	2	+
F56-7	sp-lherzolite	Adige Valley	Protogranular. Intruded by the host	57	30	10	3	+ + +
F56-8	sp-harzburgite	Adige Valley	Protogranular	89	4	4	3	+
F56-9	sp-lherzolite	Adige Valley	Protogranular	60	27	10	3	+ +
F56-10	sp-harzburgite	Adige Valley	Protogranular	65	31	3	1	+
F56-11	sp-harzburgite	Adige Valley	Protogranular	70	24	4	2	+ +
F56-13	sp-harzburgite	Adige Valley	Protogranular	75	23	1	1	+ +
F56-14	sp-harzburgite	Adige Valley	Protogranular	80	18	1	1	+ + +
F56-15	sp-harzburgite	Adige Valley	Protogranular	60	37	1	2	+
F56-16	sp-lherzolite	Adige Valley	Protogranular	61	24	10	5	+
F56-17	sp-lherzolite	Adige Valley	Protogranular. Intruded by the host	75	15	9	1	+
5Mlh*	sp-lherzolite	San Giovanni Ilarione	Protogranular to granuloblastic	75	15	8	1	+
6Mlh*	sp-lherzolite	San Giovanni Ilarione	Protogranular to granuloblastic	70	15	14	1	+
15Mlh*	sp-harzburgite	San Giovanni Ilarione	Protogranular to granuloblastic	87	12	—	1	+
36Mlh**		San Giovanni Ilarione		59	24	13	4	
28AMlh*	sp-harzburgite	Monte Purga di Bolca	Protogranular to granuloblastic	66	29	—	—	+
325Mlh*	sp-lherzolite	Monte Madarosa	Coarse-grained. Cpx shows pyrometamorphic textures	54	26	15	3	+
25AMlh**		Monte Madarosa		60	23	13	4	
25BMlh**		Monte Madarosa		48	27	22	3	
25CMlh*	sp-lherzolite	Monte Madarosa	Coarse-grained. Cpx shows pyrometamorphic textures	72	17	8	3	+
SG1XEN**	sp-lherzolite	Lessini Mts.		71	23	5	1	
SG3XEN**	sp-lherzolite	Lessini Mts.		77	13	6	4	
SG6XEN**	sp-lherzolite	Lessini Mts.		65	26	7	2	

\*Data from Morten, 1987. Modal values by visual estimation. Amount of serpentinization: + = 1–5%; ++ = 5–10%; +++ = 10–15%.

\*\*Thin section not available: mode estimated by mass balance between mineral and whole-rock compositions.

### Adige valley

Xenoliths from Adige valley consist of four-phases lherzolites and harzburgites with olivine, orthopyroxene, clinopyroxene and spinel, in order of decreasing abundances. They only show protogranular texture (Mercier and Nicolas, 1975) that is characterized by coarse olivine and orthopyroxene (>2 mm) and coarse- to medium-sized clinopyroxene and spinel (1–2 mm). Coarse olivine generally shows kink bands and pyroxene is commonly exsolved. Clinopyroxene locally occurs in interstitial positions between olivine and orthopyroxene. Spinel occurs in a variety of textural types such as holly-leaf shaped large grains, small interstitial grains and vermicular symplectite with orthopyroxene. In order to assess the geochemical fingerprint of the host basalt contamination on the xenoliths, we have also considered three samples (55B, F56-7, and F56-17) that display veinlets in physi-

cal continuity with the host basalt. Basalt or chlorite, which is interpreted as the alteration product of infiltrated basaltic glass, fills these veinlets. Serpentine is locally present along the grain boundaries of olivine and within microcracks in olivine.

### San Giovanni Ilarione (Lessini Mts.)

Xenoliths from this locality are spinel lherzolites with complex textures defined by the coexistence of protogranular and granuloblastic domains. The protogranular domain consists of strained olivine with curvilinear to irregular grain boundaries. Large orthopyroxene grains show thin exsolution lamellae of Ca-rich pyroxene whereas the pale green interstitial clinopyroxene grains carry exsolution lamellae of Ca-poor pyroxene. In the granuloblastic domain, fine-grained olivine is unstrained and shows rectilinear grain bounda-

Table 2a. Representative major element composition of olivines. Oxides expressed in wt.%. b.d.l., below detection limit; n.a., not analyzed.

	Adige Valley				Lessini Mts.*			
	56B Spl-lherz	F56-5 Spl-harz	F56-7 Spl-lherz	F56-9 Spl-lherz	15 Spl-harz	25 Spl-lherz	25C Spl-lherz	28A Spl-harz
SiO <sub>2</sub>	40.22	40.86	40.68	40.65	42.14	41.06	40.77	41.67
TiO <sub>2</sub>	0.05	0.02	0.01	b.d.l.	b.d.l.	b.d.l.	b.d.l.	b.d.l.
Al <sub>2</sub> O <sub>3</sub>	0.16	b.d.l.	b.d.l.	b.d.l.	b.d.l.	0.02	b.d.l.	0.03
Cr <sub>2</sub> O <sub>3</sub>	0.00	0.02	0.05	b.d.l.	b.d.l.	b.d.l.	b.d.l.	b.d.l.
FeO	9.82	9.12	9.68	9.77	7.83	10.04	10.15	8.79
MnO	0.19	0.18	0.08	0.11	0.13	0.15	0.13	0.08
MgO	49.51	49.31	49.79	49.57	49.97	48.48	48.12	49.58
CaO	0.05	0.02	0.05	0.03	0.05	0.06	0.07	b.d.l.
NiO	0.39	0.44	0.39	0.41	n.a.	n.a.	n.a.	n.a.
Sum	100.38	99.96	100.72	100.13	100.12	99.81	99.24	100.15
mg#	0.90	0.91	0.90	0.90	0.92	0.90	0.89	0.91

\*EPM data from Morten (1987).

Table 2b. Representative major element composition of orthopyroxenes. Oxides expressed in wt.%.

	Adige Valley						Lessini Mts.*			
	56B Spl-lherz core	56B Spl-lherz rim	F56-5 Spl-harz core	F56-7 Spl-lherz core	F56-9 Spl-lherz core	F56-9 Spl-lherz rim vs. Cpx	15 Spl-harz	25 Spl-lherz	25C Spl-lherz	28A Spl-harz
SiO <sub>2</sub>	54.62	55.96	55.54	55.26	54.93	55.58	58.08	54.97	54.99	56.15
TiO <sub>2</sub>	0.11	0.14	0.02	0.15	0.11	0.11	b.d.l.	0.11	0.10	0.04
Al <sub>2</sub> O <sub>3</sub>	4.58	4.70	3.16	3.93	3.58	4.37	1.75	4.89	4.34	3.53
Cr <sub>2</sub> O <sub>3</sub>	0.24	0.31	0.44	0.31	0.23	0.31	0.56	0.45	0.60	0.47
FeO	6.17	6.32	6.17	6.38	6.07	6.06	5.16	6.46	6.24	5.48
MnO	0.14	0.14	0.15	0.22	0.15	0.12	0.08	0.17	0.17	0.15
MgO	32.55	33.48	34.18	33.57	33.76	33.81	33.83	31.85	32.97	33.53
CaO	0.78	0.51	0.52	0.59	0.44	0.43	0.85	0.78	0.53	0.77
Na <sub>2</sub> O	0.11	0.04	0.06	0.10	0.06	0.02	0.06	0.09	0.05	0.12
Sum	99.32	101.60	100.24	100.50	99.34	100.80	100.37	99.77	99.99	100.24
mg#	0.90	0.90	0.91	0.90	0.91	0.91	0.92	0.90	0.90	0.92
Equilibration temperatures (°C)										
Wells	914	821	909	956	952	847		998	926	
Ta97	836	704	842	888	881	756		969	883	

Temperature estimates are from Wells (1977) and the two-pyroxene geothermometer of Taylor (1997), using the clinopyroxene compositions of Table 2c. Assumed pressure is 1.5 GPa. \*EPM data from Morten (1987).

ries. Pyroxenes do not show exsolution lamellae. Brown spinel (Morten *et al.*, 1989) occurs in a variety of textural positions: (1) as holly-leaf grains, (2) as interstitial grains associated with olivine and glassy patches and (3) as vermicular grains (“wormy spinels”) forming a symplectitic intergrowth with orthopyroxenes and, to a minor extent, with clinopyroxene. The wormy spinels are likely exsolved from pyroxenes (Morten *et al.*, 1989) according to the reaction  $(2\text{Mg}_2\text{SiO}_4 + 2\text{MgCrAlSiO}_6)_{\text{ss}} = 2\text{MgMgSi}_2\text{O}_6 + (\text{MgCr}_2\text{O}_4 + \text{MgAl}_2\text{O}_4)_{\text{ss}}$  proposed by Garrison and Taylor (1981). If we consider the Ringwood

(1975) phase diagram in the MgO-Al<sub>2</sub>O<sub>3</sub>-SiO<sub>2</sub> system, the above reaction requires a temperature decrease and allows the transition from a spinel-absent, olivine + pyroxene peridotite field to the spinel-peridotite field.

#### Monte Madarosa (Lessini Mts.)

Spinel-lherzolites from this locality show reactions at the contact with the host basalt and small basaltic veinlets that have partly invaded the xenoliths. The inner portions, i.e. far from the xenolith-host basalt contact, show coarse-grained texture. Olivines generally show undulose extinc-

Table 2c. Representative major element composition of clinopyroxenes. Oxides expressed in wt.%.

	Adige Valley						Lessini Mts.*	
	56B Spl-lherz rim vs. Opx	56B Spl-lherz core	F56-5 Spl-lherz core	F56-7 Spl-lherz core	F56-9 Spl-lherz rim vs. Opx	F56-9 Spl-lherz core	25 Spl-lherz	25C Spl-lherz
SiO <sub>2</sub>	51.39	51.60	53.02	52.32	53.03	51.82	50.94	52.01
TiO <sub>2</sub>	0.55	0.71	0.14	0.50	0.40	0.40	0.45	0.20
Al <sub>2</sub> O <sub>3</sub>	6.19	6.29	4.01	5.99	5.53	5.86	5.15	4.91
Cr <sub>2</sub> O <sub>3</sub>	0.80	0.72	0.87	0.92	0.96	0.88	1.02	1.47
FeO	3.14	2.93	2.71	2.78	2.49	2.46	3.20	2.94
MnO	0.01	0.06	0.05	0.04	0.11	0.11	0.02	0.06
MgO	15.09	14.90	16.28	15.01	14.97	14.52	16.04	15.30
CaO	21.03	21.07	21.98	20.48	21.77	21.53	21.88	22.70
Na <sub>2</sub> O	1.47	1.56	1.13	1.68	1.60	1.80	0.52	0.57
Sum	99.67	99.84	100.19	99.72	100.87	99.37	99.22	100.16
mg#	0.90	0.90	0.91	0.91	0.91	0.91	0.90	0.90

\*EPM data from Morten (1987).

Table 2d. Representative major element composition of spinels. Oxides expressed in wt.%. n.a., not analyzed.

	Adige Valley				Lessini Mts.*	
	56B Spl-lherz vermicular in Opx	F56-7 Spl-lherz vermicular in Opx	F56-9 Spl-lherz disseminated grain, core	F56-9 Spl-lherz disseminated grain, rim	15 Spl-lherz	25 Spl-lherz
TiO <sub>2</sub>	0.19	0.17	0.08	0.07	0.09	0.12
Al <sub>2</sub> O <sub>3</sub>	56.00	52.02	52.90	53.24	14.11	58.08
Cr <sub>2</sub> O <sub>3</sub>	9.31	13.11	13.32	12.74	53.56	9.73
FeO	12.51	13.61	12.46	12.29	17.85	12.55
MnO	0.10	0.15	0.09	0.04	0.03	0.14
MgO	20.53	20.04	19.80	19.68	14.23	20.62
NiO	0.38	0.35	0.30	0.45	n.a.	n.a.
Sum	99.01	99.44	98.96	98.52	99.87	101.24
mg#	0.75	0.72	0.74	0.74	0.59	0.75
cr#	0.10	0.14	0.14	0.14	0.72	0.10

\*EPM data from Morten (1987).

tion and orthopyroxenes display exsolution lamellae. The latter commonly show reaction rims against olivine and clinopyroxene. These rims consist of fine-grained olivines and clinopyroxenes set in a glassy matrix. More importantly, these rims and the host basalts are not in contact. Two types of clinopyroxenes occur. The first, less abundant than the second, is made of large anhedral grains with exsolution lamellae. The second type comprises clinopyroxenes with spongy appearance because of the presence of fine glass inclusions. Spinel occurs as holly-leaf shaped grains, whereas spinels in contact with the host basalt show opaque, Cr-enriched rims. The reaction zones along the contact between xenoliths and the host basalt consist of fine olivine and clinopyroxene(±glass) aggregates, which replace former pyroxenes. In the reaction zones, large olivines with embayed grains also oc-

cur. Rarely, these olivines show reaction rims consisting of fine-grained olivine plus glass.

#### Monte Purga di Bolca (Lessini Mts.)

Ultramafic xenoliths from Monte Purga di Bolca site mainly show porphyroclastic textures, with large olivine, up to 2 mm, and subordinate orthopyroxene porphyroclasts that set up in a fine-grained (100–400 μm) matrix formed mainly of olivine. The olivine porphyroclasts are strained with undulose extinction whereas the olivine neoblasts are unstrained. Orthopyroxene shows exsolution lamellae of Ca-rich pyroxene. Fine (0.4–0.6 mm) interstitial clinopyroxene grains are partly or totally spongy. The spinels are present as brown grains with reaction rims at the contacts with spongy clinopyroxene and olivine.

## ANALYTICAL METHODS

Major element compositions of the mineral phases were analyzed by electron microprobe with a Cameca CAMEBAX (IGG-CNR, Padova), equipped with four wavelength-dispersive spectrometers. Natural silicates and oxides were used as standards. The accelerating potential employed was 15 kV with a beam current of 10 nA and a beam size of about 1  $\mu\text{m}$  diameter. Peak counting was 10 seconds. Raw data were corrected on line for matrix effects with the ZAF routine.

Thirty spinel peridotites, together with six host lavas from the Adige Valley and Lessini Mts. were analyzed for major and trace elements, and Sr, Nd, Pb and O isotopic compositions. Among the peridotites, only three samples (55B, F56-7, and F56-17) are intruded by veinlets of the basanite host; the other xenoliths are fresh and with no petrographical evidence of interaction with host material. Whole-rock X-ray fluorescence (XRF) analyses of major elements were determined at the Earth Science Department of Pisa University, using a PHILIPS PW 1480 spectrometer and following the analytical procedures of Franzini *et al.* (1975) and Leoni and Saitta (1976). Trace element concentrations were obtained at the CRPG in Nancy (Alibert *et al.*, 1983). Ferrous/ferric iron ratios were determined by titration. Whole-rock chemical separation of Sr, Nd and Pb has been achieved at the Laboratory of Tectonophysique of the Université of Montpellier II (France). All samples were leached prior to dissolution in 2.5N HCl for 30 minutes at 60°C in sealed beakers. Sr and Nd isotopic composition were analyzed by the multi-collector Finnigan Mat mass spectrometer of the University Paul Sabatier of Toulouse (France) and normalized to  $^{86}\text{Sr}/^{88}\text{Sr} = 0.1194$  and  $^{146}\text{Nd}/^{144}\text{Nd} = 0.7219$ .  $^{87}\text{Sr}/^{86}\text{Sr}$  values of the NBS-987 Sr standard during the analytical session were  $0.710250 \pm 15$  ( $2\sigma$ , external reproducibility) on 11 standard determinations. The  $^{143}\text{Nd}/^{144}\text{Nd}$  of the La Jolla Nd standard was  $0.511850 \pm 12$  ( $2\sigma$ , external reproducibility) on 12 standard determinations. Pb chemical purifications were done according to a slightly modified procedure of Manhès *et al.* (1978) and White and Dupré (1986). Pb isotope compositions were determined by multi-collector magnetic-sector inductively-coupled-plasma mass spectrometry, using the VG model Plasma 54 in Lyon (White *et al.*, 2000). Total procedural blanks for Sr, Nd, and Pb were better than 100, 8 and 25 pg, respectively. Sample to blank ratios for all three elements for all samples analyzed were  $> 1000$ . The whole-rock (WR)  $\delta^{18}\text{O}$  values have been obtained by gas mass spectrometry at Activation Laboratories of Ancaster (Ontario). Stated precision of analyses is 0.3‰. The isotopic composition of a sample is given as:  $\delta_{\text{sample}} = (R_{\text{sample}}/R_{\text{standard}} - 1) * 1000$  in per mil unit, where R is  $^{18}\text{O}/^{16}\text{O}$  and the standard is SMOW.

## MINERAL CHEMISTRY AND TEMPERATURE ESTIMATES

Representative compositions (major element) of minerals are summarized in Table 2(a)–(d). Olivine shows small compositional variations, with a mg# [=molar MgO/(MgO + FeO<sub>tot</sub>)], varying from 0.89 to 0.92 and very low CaO contents (below 0.07 wt.%). Orthopyroxenes are enstatites with a mg# of 0.90–0.92. The orthopyroxenes from the Adige Valley display CaO and Cr<sub>2</sub>O<sub>3</sub> contents that are lower than those of orthopyroxenes from the Lessini Mts. xenoliths. Among the other oxides, the concentration of Al<sub>2</sub>O<sub>3</sub> is significant and varies from 1.75 wt.% to 4.89 wt.%, whereas the TiO<sub>2</sub> content is low (0.02–0.15 wt.%). Clinopyroxenes from both the localities are Cr-diopsides with no significant mg# variations, TiO<sub>2</sub> ranging between 0.14–0.71 wt.% and Al<sub>2</sub>O<sub>3</sub> between 4.01–6.29 wt.%. The clinopyroxenes from the Adige Valley display lower Cr<sub>2</sub>O<sub>3</sub> and higher Na<sub>2</sub>O contents than the clinopyroxenes from the Lessini Mts. xenoliths. Spinel from the Adige Valley show restricted ranges in mg# and cr# [molar Cr<sub>2</sub>O<sub>3</sub>/(Cr<sub>2</sub>O<sub>3</sub> + Al<sub>2</sub>O<sub>3</sub>)] whereas those from the Lessini Mts. show different composition as a function of the degree of fertility of the peridotite. The sample 15 Mlh is a harzburgite and contains chromium- and iron-rich spinels (cr# = 0.74, mg# = 0.59). Conversely, spinels from the sample 25 Mlh (a spinel-lherzolite) are highly magnesian and chromium-poor (mg# = 0.75; cr# = 0.10). Morten (1987) and Morten *et al.* (1989) provided a detailed mineral chemistry description of the spinels from the Lessini Mts. xenoliths and here we report the major conclusions. Spinel from the Lessini Mts. xenoliths have mg# and cr# that vary as a function of their textural site. Interstitial spinels, which are surrounded by silicates, show a restricted range of mg# (0.75–0.81) and cr# (0.09–0.15). On the other hand, spinels in contact with glass sites show a negative correlation between mg# and cr#, with large variations in mg# (0.23–0.74) and relatively limited changes in cr# (0.09–0.35). This trend was interpreted as the result of a combination of partial melting, solid-liquid and subsolidus reactions.

Equilibration temperatures were calculated using the Wells (1977) and the Taylor (1998) geothermometers. In these calculations we used an input pressure of 1.5 GPa, which is assumed to represent an average pressure for mantle xenoliths equilibrated in the spinel-facies. The two geothermometers yield similar values only at the high-temperature end of the dataset. The discrepancy between the two methods is largest ( $>100^\circ\text{C}$ ) for the spinel-harzburgite 56B, which records the lowest temperature. In general, the Adige Valley xenoliths give equilibration temperatures somewhat lower than the Lessini Mts. xenoliths. In the Adige Valley xenoliths, the temperatures calculated from the pyroxene rim compositions are lower of about 100°C in comparison with the temperature esti-

Table 3a. Whole-rock major element abundances (wt.% oxides) for the VVP xenoliths and host basanites. mg# and cr# are calculated as  $[100 * Mg / (Mg + Fe)]$  and  $[100 * Cr / (Cr + Al)]$  respectively.

Sample	Lithotype	Locality	mg#	cr#	SiO <sub>2</sub>	TiO <sub>2</sub>	Al <sub>2</sub> O <sub>3</sub>	Fe <sub>2</sub> O <sub>3</sub>	FeO	MnO	MgO	CaO	Na <sub>2</sub> O	K <sub>2</sub> O	P <sub>2</sub> O <sub>5</sub>	LOI	Total
55B	sp-lherzburgite	Adige Valley	89	11	39.64	0.25	2.06	4.93	3.34	0.13	36.85	2.42	0.01	0.07	0.28	10.02	100.00
56B	sp-lherzolitite	Adige Valley	89	8	42.78	0.12	2.15	3.29	5.28	0.13	37.48	4.78	0.05	0.05	0.02	3.88	100.01
F56-1	sp-lherzolitite	Adige Valley	90	5	44.06	0.18	3.49	2.11	5.71	0.13	36.81	3.73	0.10	0.05	0.07	3.56	100.00
F56-2A	sp-lherzolitite	Adige Valley	89	6	42.50	0.15	2.72	3.32	5.14	0.13	37.30	4.98	0.05	0.04	0.07	3.63	100.03
F56-2B	sp-lherzolitite	Adige Valley	90	12	43.88	0.09	2.16	1.91	5.79	0.12	41.25	1.94	0.05	0.08	0.03	3.17	100.47
F56-3	sp-lherzburgite	Adige Valley	91	11	43.88	0.09	2.16	1.91	5.79	0.12	41.25	1.94	0.05	0.08	0.03	2.70	100.00
F56-4	sp-lherzolitite	Adige Valley	90	7	42.28	0.13	3.47	2.38	4.98	0.12	36.33	4.59	0.05	0.14	0.07	5.45	99.99
F56-5	sp-lherzburgite	Adige Valley	91	17	43.38	0.02	1.21	1.93	6.09	0.13	43.42	1.17	0.00	0.02	0.01	2.64	100.02
F56-7	sp-lherzburgite	Adige Valley	90	6	42.62	0.13	3.52	1.97	5.85	0.13	37.45	3.19	0.10	0.31	0.46	4.28	100.01
F56-8	sp-lherzolitite	Adige Valley	90	8	43.68	0.11	2.65	2.26	5.38	0.13	39.33	2.93	0.08	0.11	0.01	3.34	100.01
F56-9	sp-lherzolitite	Adige Valley	90	7	44.33	0.14	2.90	1.99	5.78	0.13	39.33	2.85	0.10	0.08	0.05	2.31	99.99
F56-10	sp-lherzburgite	Adige Valley	90	10	43.38	0.06	1.76	2.09	6.02	0.13	41.89	1.37	0.00	0.05	0.01	3.25	100.01
F56-11	sp-lherzburgite	Adige Valley	91	15	43.65	0.04	1.65	1.62	6.30	0.13	42.86	1.13	0.00	0.05	0.01	2.56	100.00
F56-13	sp-lherzburgite	Adige Valley	91	12	43.41	0.04	1.68	2.19	5.72	0.12	42.58	1.34	0.00	0.07	0.02	2.84	100.01
F56-14	sp-lherzburgite	Adige Valley	91	13	43.23	0.05	1.66	1.87	5.92	0.12	42.28	1.52	0.00	0.01	0.01	3.33	100.00
F56-15	sp-lherzburgite	Adige Valley	91	14	43.63	0.03	1.34	1.79	6.28	0.12	43.22	0.84	0.00	0.04	0.01	2.98	100.28
F56-16	sp-lherzolitite	Adige Valley	89	6	43.73	0.16	3.79	1.66	6.41	0.13	37.41	3.55	0.16	0.16	0.03	2.81	100.00
F56-17	sp-lherzolitite	Adige Valley	90	7	43.30	0.21	3.84	1.66	5.65	0.12	36.60	3.42	0.31	0.26	0.19	4.44	100.00
5Mlh	sp-lherzolitite	Lessini Mts.	90	13	44.39	—	2.12	8.67*	—	0.13	40.94	2.33	0.20	0.06	0.14	1.12	100.10
6Mlh	sp-lherzolitite	Lessini Mts.	90	8	44.94	0.09	3.43	8.56*	—	0.13	37.64	3.69	0.26	0.10	0.10	1.19	100.13
15Mlh	sp-lherzolitite	Lessini Mts.	92	20	43.51	—	0.69	8.07*	—	0.11	46.60	0.41	—	—	0.08	0.97	100.44
36Mlh	sp-lherzolitite	Lessini Mts.	89	8	43.09	0.16	3.80	9.37*	—	0.13	38.29	3.37	0.21	0.06	0.16	1.40	100.04
28AMlh	sp-lherzolitite	Lessini Mts.	90	12	43.84	0.07	2.28	8.87*	—	0.13	42.35	1.22	0.23	0.17	0.11	0.63	99.90
25Mlh	sp-lherzolitite	Lessini Mts.	89	8	44.11	0.12	4.66	9.05*	—	0.13	37.12	3.14	0.29	0.09	0.07	0.54	99.32
25AMlh	sp-lherzolitite	Lessini Mts.	89	8	43.37	0.10	3.47	9.31*	—	0.13	40.03	2.72	0.16	—	0.08	0.44	99.81
25BMlh	sp-lherzolitite	Lessini Mts.	90	8	45.33	0.15	3.53	8.12*	—	0.12	35.42	4.63	0.37	0.13	0.07	1.09	98.96
25CMlh	sp-lherzolitite	Lessini Mts.	90	13	42.10	0.10	2.51	9.60*	—	0.14	41.83	1.77	0.23	0.17	0.15	1.10	99.70
SG1XEN	sp-lherzolitite	Lessini Mts.	90	8	43.63	0.08	1.98	1.72	6.75	0.13	42.86	1.39	0.15	0.04	0.03	0.50	99.26
SG3XEN	sp-lherzolitite	Lessini Mts.	91	6	41.41	0.13	3.08	0.08	7.32	0.13	43.57	1.91	0.30	0.16	0.05	1.05	99.19
SG6XEN	sp-lherzolitite	Lessini Mts.	90	9	44.13	0.10	2.49	0.97	7.22	0.13	41.40	2.02	0.16	0.05	0.02	0.51	99.20
5MB	basanite	Lessini Mts.	60	0.23	42.45	2.98	12.91	13.36*	—	0.19	11.12	10.49	3.06	1.77	1.09	1.01	100.43
6MB	basanite	Lessini Mts.	62	0.23	42.17	2.92	12.8	13.37*	—	0.19	11.39	10.36	3.11	1.63	0.99	1.04	100.13
27MB	basanite	Lessini Mts.	60	0.25	42.94	3.01	12.89	13.49*	—	0.17	11.17	11.54	2.93	0.9	0.66	0.53	100.23
28MB	basanite	Lessini Mts.	65	0.37	41.87	3.06	12.02	13.40*	—	0.18	13.67	10.33	2.62	1.63	0.87	0.66	100.31
25MB	basanite	Lessini Mts.	60	0.26	42.15	2.85	12.88	13.29*	—	0.19	11.05	10.84	3.1	1.59	0.98	1.09	100.01
56MB <sup>a)</sup>	basanite	Adige Valley	59	0.20	37.91	2.77	11.97	6.13	7.12	0.14	10.14	15.33	2.92	0.83	—	4.46	99.72

\*Fe<sub>2</sub>O<sub>3</sub> tot.

<sup>a)</sup>Morten (1987).

Table 3b. Whole-rock trace element abundances (ppm) for the VVP xenoliths and host lavas. Precision for trace element analyses is about 5–20% at 1 ppm level, about 2–10% at 10 ppm level and about 2–5% at 100 ppm level.

Sample	Lithotype	Locality	Ni	Co	Cr	V	Rb	Sr	Ba	Zr	Y	Nb	Ta	La	Ce	Pr
55B	sp-harzburgite	Adige Valley	1569	95	2973	55.5	2.88	124	123	33.3	4.96	9.80	0.47	15.0	29.5	3.41
56B	sp-lherzolite	Adige Valley	1992	101	2013	64.3	1.51	66.1	21	7.01	2.62	0.56	0.03	1.26	2.56	0.31
F56-1	sp-lherzolite	Adige Valley	1624	94	2244	75.4	1.94	27.1	17	14.1	3.79	1.99	0.11	2.43	5.09	0.58
F56-2A	sp-lherzolite	Adige Valley	2259	97	2627	70.7	1.11	27.1	10	9.19	3.13	0.88	0.07	1.46	2.88	0.33
F56-2B	sp-lherzolite	Adige Valley	2178	107	2834	57.9	0.96	26.0	5	4.32	2.15	0.25	b.d.l.	0.29	0.58	0.10
F56-3	sp-harzburgite	Adige Valley	1925	106	2788	56.1	2.79	25.3	8	7.38	1.77	1.27	0.07	1.82	3.70	0.39
F56-4	sp-lherzolite	Adige Valley	1747	97	2958	73.5	5.79	71.6	35	11.6	3.70	2.13	0.10	4.70	10.2	1.10
F56-5	sp-harzburgite	Adige Valley	2244	116	2690	47.1	b.d.l.	9.28	b.d.l.	0.84	0.52	0.14	b.d.l.	0.93	1.42	0.13
F56-7	sp-harzburgite	Adige Valley	1847	106	2648	50.8	8.84	73.7	27	39.6	4.82	15.04	0.56	7.44	17.8	2.17
F56-8	sp-lherzolite	Adige Valley	1738	98	2364	67.1	3.74	24.1	18	7.68	2.81	0.89	0.05	1.38	2.69	0.28
F56-9	sp-lherzolite	Adige Valley	2042	100	2488	71.0	2.72	70.3	11	12.2	3.30	1.53	0.07	1.64	3.38	0.42
F56-10	sp-harzburgite	Adige Valley	2178	103	2269	48.3	1.76	12.8	6	3.99	1.25	0.37	b.d.l.	0.53	1.37	0.15
F56-11	sp-harzburgite	Adige Valley	2157	108	3186	46.0	1.51	17.2	7	2.16	0.89	0.27	b.d.l.	1.47	2.72	0.30
F56-13	sp-harzburgite	Adige Valley	2373	110	2646	39.3	2.01	20.2	5	9.76	0.97	1.67	0.11	1.53	3.15	0.35
F56-14	sp-harzburgite	Adige Valley	2177	108	2833	55.0	b.d.l.	4.47	b.d.l.	1.50	1.25	0.11	b.d.l.	0.11	0.22	b.d.l.
F56-15	sp-harzburgite	Adige Valley	2252	111	2436	38.4	1.24	13.4	4.09	1.26	0.74	0.20	b.d.l.	1.17	2.27	0.22
F56-16	sp-lherzolite	Adige Valley	1907	102	2714	68.1	4.94	78.1	41.9	17.9	3.78	2.83	0.14	6.07	12.23	1.22
F56-17	sp-lherzolite	Adige Valley	1940	95	3492	61.2	8.97	122	69.8	39.2	4.24	10.65	0.53	7.78	16.80	1.97
5Mlh	sp-lherzolite	Lessini Mts.	2198	106	3152	46.0	2.77	49.0	26.5	8.49	1.86	1.522	0.10	2.38	5.70	0.64
6Mlh	sp-lherzolite	Lessini Mts.	1895	99	3049	85.8	4.41	20.4	9.62	3.81	3.19	0.914	0.06	0.68	1.66	0.14
15Mlh	sp-lherzolite	Lessini Mts.	2642	117	1728	18.2	0.76	5.39	b.d.l.	3.98	0.42	1.081	0.07	0.98	2.24	0.19
36Mlh	sp-lherzolite	Lessini Mts.	2028	107	3153	80.1	3.18	14.6	8.85	9.13	3.68	1.806	0.12	2.44	5.27	0.54
28AMlh	sp-lherzolite	Lessini Mts.	2121	109	3228	46.4	3.94	51.7	17.0	9.76	1.48	3.215	0.12	1.60	4.28	0.46
25Mlh	sp-lherzolite	Lessini Mts.	1975	103	3952	89.4	3.10	32.1	25.8	4.96	3.21	0.923	0.06	1.40	3.07	0.31
25AMlh	sp-lherzolite	Lessini Mts.	2178	113	2904	72.2	1.72	14.6	18.4	3.14	2.87	0.403	0.03	0.47	1.28	0.12
25BMlh	sp-lherzolite	Lessini Mts.	1665	91	3150	93.2	4.98	48.0	24.2	7.41	4.02	1.576	0.13	1.46	3.29	0.32
25CMlh	sp-lherzolite	Lessini Mts.	2332	122	3891	44.1	5.43	193	72.5	14.3	2.19	3.518	0.21	5.49	9.65	0.92
SG1XEN	sp-lherzolite	Lessini Mts.	2081	118	1757	48.8	1.19	15.0	8.00	4.00	1.54	0.68	0.04	0.69	1.18	0.15
SG3XEN	sp-lherzolite	Lessini Mts.	1896	122	2042	56.9	4.28	32.0	21.0	16.0	2.67	3.42	0.21	2.60	4.78	0.52
SG6XEN	sp-lherzolite	Lessini Mts.	1886	111	2516	57.8	1.35	10.0	b.d.l.	7.00	2.16	0.54	0.03	0.63	1.67	0.27
5MB	basanite	Lessini Mts.	259	55	304	243	39.5	937	807	258	28.6	63.8	4.26	68.6	131	14.7
6MB	basanite	Lessini Mts.	282	57	312	242	38.1	943	799	254	28.9	61.9	4.25	67.8	129	14.5
27MB	basanite	Lessini Mts.	255	60	328	269	18.0	662	330	171	23.5	34.7	2.53	35.3	75.1	9.24
28MB	basanite	Lessini Mts.	371	60	453	242	30.7	801	426	223	24.8	53.0	3.76	41.3	89.7	10.9
25MB	basanite	Lessini Mts.	245	55	343	243	37.0	960	824	241	28.8	60.8	4.05	67.7	129	14.5
56MB <sup>a)</sup>	basanite	Adige Valley	187	60	250	223	—	—	—	—	—	—	—	69	114	—

<sup>a)</sup>Morten, 1987; b.d.l. = below detection limit.

Sample	Lithotype	Locality	Nd	Sm	Eu	Gd	Tb	Dy	Ho	Er	Tm	Yb	Lu	Hf	Th	U	Pb
55B	sp-harzburgite	Adige Valley	12.5	2.27	0.68	1.72	0.24	1.14	0.19	0.46	0.06	0.38	0.05	0.61	1.68	0.45	1.02
56B	sp-lherzolite	Adige Valley	1.29	0.36	0.13	0.39	0.06	0.43	0.10	0.26	0.04	0.29	0.05	0.19	0.11	b.d.l.	b.d.l.
F56-1	sp-lherzolite	Adige Valley	2.51	0.56	0.22	0.58	0.10	0.59	0.12	0.33	0.05	0.33	0.05	0.31	0.35	0.12	b.d.l.
F56-2A	sp-lherzolite	Adige Valley	1.41	0.37	0.14	0.46	0.08	0.54	0.11	0.32	0.05	0.35	0.06	0.20	0.19	b.d.l.	b.d.l.
F56-2B	sp-lherzolite	Adige Valley	0.53	0.17	0.07	0.28	0.05	0.33	0.07	0.21	0.04	0.24	0.04	0.11	b.d.l.	b.d.l.	b.d.l.
F56-3	sp-harzburgite	Adige Valley	1.62	0.37	0.13	0.36	0.06	0.27	0.07	0.18	0.03	0.15	0.03	0.16	0.21	b.d.l.	b.d.l.
F56-4	sp-lherzolite	Adige Valley	4.24	0.86	0.27	0.75	0.11	0.64	0.13	0.34	0.05	0.34	0.05	0.27	0.52	0.14	b.d.l.
F56-5	sp-harzburgite	Adige Valley	0.52	0.06	0.02	b.d.l.	b.d.l.	0.06	0.02	0.06	0.01	0.10	0.01	b.d.l.	0.13	b.d.l.	b.d.l.
F56-7	sp-harzburgite	Adige Valley	9.20	1.99	0.62	1.61	0.24	1.05	0.18	0.39	0.06	0.29	0.05	0.65	0.80	0.22	b.d.l.
F56-8	sp-lherzolite	Adige Valley	1.16	0.30	0.12	0.39	0.06	0.43	0.10	0.26	0.04	0.30	0.05	0.22	0.11	b.d.l.	b.d.l.
F56-9	sp-lherzolite	Adige Valley	1.87	0.47	0.20	0.54	0.08	0.54	0.12	0.35	0.05	0.32	0.05	0.28	0.25	b.d.l.	b.d.l.
F56-10	sp-harzburgite	Adige Valley	0.70	0.17	0.07	0.24	0.03	0.18	0.06	0.12	0.02	0.13	0.03	0.07	b.d.l.	b.d.l.	b.d.l.
F56-11	sp-harzburgite	Adige Valley	0.95	0.14	0.06	0.13	0.02	0.09	0.03	0.08	0.02	0.11	0.01	b.d.l.	0.14	b.d.l.	b.d.l.
F56-13	sp-harzburgite	Adige Valley	1.46	0.26	0.10	0.23	0.03	0.19	0.04	0.07	0.01	0.11	0.02	0.17	0.14	b.d.l.	b.d.l.
F56-14	sp-harzburgite	Adige Valley	0.11	0.11	0.03	0.13	0.03	0.17	0.05	0.09	0.02	0.13	0.02	b.d.l.	b.d.l.	b.d.l.	b.d.l.
F56-15	sp-harzburgite	Adige Valley	0.73	0.13	0.04	b.d.l.	0.02	0.08	0.02	0.08	0.01	0.11	0.02	b.d.l.	0.11	b.d.l.	b.d.l.
F56-16	sp-lherzolite	Adige Valley	4.48	0.78	0.27	0.76	0.11	0.65	0.13	0.35	0.05	0.33	0.05	0.39	1.00	0.21	b.d.l.
F56-17	sp-lherzolite	Adige Valley	8.62	1.65	0.53	1.15	0.18	0.95	0.15	0.37	0.05	0.26	0.04	0.71	0.95	0.25	b.d.l.
5Mh	sp-lherzolite	Lessini Mts.	2.48	0.49	0.15	0.44	0.06	0.35	0.07	0.18	0.03	0.19	0.03	0.15	0.29	0.08	1.89
6Mh	sp-lherzolite	Lessini Mts.	0.66	0.22	0.09	0.34	0.07	0.49	0.11	0.35	0.06	0.39	0.06	0.13	0.16	b.d.l.	1.84
15Mh	sp-lherzolite	Lessini Mts.	0.68	0.12	0.03	0.11	0.01	0.08	0.01	b.d.l.	b.d.l.	0.04	b.d.l.	0.07	0.21	b.d.l.	2.51
36Mh	sp-lherzolite	Lessini Mts.	2.19	0.53	0.19	0.60	0.10	0.62	0.13	0.36	0.06	0.39	0.06	0.25	0.40	0.13	2.36
28AMh	sp-lherzolite	Lessini Mts.	1.80	0.39	0.13	0.34	0.05	0.28	0.05	0.13	0.02	0.15	0.02	0.17	0.17	b.d.l.	2.04
25Mh	sp-lherzolite	Lessini Mts.	1.15	0.32	0.11	0.42	0.08	0.52	0.11	0.34	0.05	0.37	0.06	0.16	0.25	0.08	1.96
25AMh	sp-lherzolite	Lessini Mts.	0.66	0.24	0.10	0.34	0.07	0.46	0.10	0.31	0.05	0.34	0.05	0.14	b.d.l.	b.d.l.	4.12
25BMh	sp-lherzolite	Lessini Mts.	1.31	0.41	0.15	0.54	0.10	0.68	0.14	0.43	0.07	0.44	0.08	0.20	0.37	0.12	3.09
25CMh	sp-lherzolite	Lessini Mts.	3.25	0.55	0.18	0.49	0.07	0.41	0.07	0.21	0.03	0.21	0.04	0.24	0.80	0.23	2.64
SG1XEN	sp-lherzolite	Lessini Mts.	0.52	0.22	0.07	0.25	0.04	0.23	0.05	0.14	0.03	0.18	0.03	0.12	0.12	b.d.l.	b.d.l.
SG3XEN	sp-lherzolite	Lessini Mts.	2.01	0.51	0.16	0.47	0.08	0.45	0.10	0.25	0.04	0.26	0.04	0.33	0.52	0.14	b.d.l.
SG6XEN	sp-lherzolite	Lessini Mts.	1.25	0.35	0.12	0.30	0.05	0.35	0.07	0.19	0.03	0.23	0.04	0.14	b.d.l.	b.d.l.	b.d.l.
5MB	basanite	Lessini Mts.	56.6	10.8	3.29	8.83	1.20	6.18	1.04	2.53	0.33	2.05	0.30	5.66	11.6	2.77	8.59
6MB	basanite	Lessini Mts.	55.6	10.5	3.27	8.81	1.19	6.17	1.01	2.51	0.32	2.06	0.30	5.65	11.3	2.74	9.26
27MB	basanite	Lessini Mts.	38.3	8.18	2.67	7.19	0.99	5.12	0.85	2.04	0.27	1.58	0.23	4.17	3.84	1.09	3.39
28MB	basanite	Lessini Mts.	44.8	9.19	2.97	7.87	1.08	5.54	0.91	2.09	0.26	1.54	0.21	5.27	4.57	1.33	3.91
25MB	basanite	Lessini Mts.	55.7	10.4	3.15	8.78	1.19	5.99	1.03	2.61	0.33	2.03	0.29	5.27	11.8	2.78	8.24
56MB	basanite	Adige Valley	52	11	3.7	—	1.3	—	—	—	—	1.8	0.29	—	—	—	—

mates using the pyroxene cores. This drop in temperature may indicate a cooling stage along the conductive geotherm before the entrainment of the Adige Valley xenoliths into the ascending basanite host. Conversely, the Lessini Mts. xenoliths record higher temperatures that might indicate a metamorphic equilibration at deep levels of the local mantle column.

### WHOLE-ROCK GEOCHEMISTRY

Major and trace element compositions of the VVP xenoliths are listed in Table 3(a) and (b).

#### *Major element composition*

The VVP xenoliths belong to the Cr-Diopside suite (defined as having mg# = 89–92, Table 3(a); Wilshire and Shervais, 1975). Their mg# (89–92) and cr# (5–20) values (Fig. 2a) are comparable to those of other Cenozoic ultramafic xenoliths entrapped in basalts from French Massif Central (Zangana *et al.*, 1999; Lenoir *et al.*, 2000), Germany (Hartmann and Wedepohl, 1990; Witt-Eickschen, 1993), Hungary (Downes *et al.*, 1992), Romania (Vaselli *et al.*, 1995), Russia (Ionov *et al.*, 1995), Mongolia (Wiechert *et al.*, 1997), China (Qi *et al.*, 1995; Chen *et al.*, 2001) and Canadian Cordillera (Peslier *et al.*, 2002). When compared to xenoliths from different geodynamic settings, such as oceanic or continental environments (Canary Islands: Wulff-Pedersen *et al.*, 1996; Neumann *et al.*, 2002; Kerguelen Islands: Grégoire *et al.*, 1997; Australia: O'Reilly and Griffin, 1988; Yaxley *et al.*, 1991; Foden *et al.*, 2002) or typical subduction zones (Marianas: Parkinson and Pearce, 1998; Papua New Guinea: Franz *et al.*, 2002; Philippines: Maury *et al.*, 1992), the VVP and French Massif Central, Germany, Hungary, Romania, Russia, China, Mongolia and Canadian Cordillera xenoliths display lower cr# values, while showing the same range of mg#, that are comparable to the primordial mantle values (Fig. 2a). This correlation likely reflects a rather fertile nature of the mantle region, eventually related to influx of deep mantle material in the lithospheric mantle.

As with the xenoliths from French Massif Central, Germany, Hungary, Romania, Russia, Mongolia, China, Canadian Cordillera and Vulture, the VVP spinel-peridotite xenoliths show a general trend of depletion in fusible basaltic components, such as TiO<sub>2</sub>, Al<sub>2</sub>O<sub>3</sub> and CaO (Figs. 2b, c, d), and a concomitant decrease of mg# from strongly depleted to relatively fertile samples (Fig. 2a). Most have lower overall TiO<sub>2</sub>, Al<sub>2</sub>O<sub>3</sub>, CaO, Na<sub>2</sub>O and higher MgO contents than the primordial mantle composition (McDonough, 1990). Most of the VVP xenoliths characterized by MgO > 38 wt.% ca. shows relatively good negative correlations for TiO<sub>2</sub>, Al<sub>2</sub>O<sub>3</sub>, and CaO vs. MgO contents, while the xenoliths with MgO = 36–39

wt.% ca. do not define any correlation trends in the same co-variation diagrams (Figs. 2b, c, d). Two of the three xenoliths, 55B and F56-17, which are contaminated by intruded veinlets of basalt, tend to have higher concentrations of the most fusible components (e.g., TiO<sub>2</sub>) than most of the other xenoliths (Figs. 2b, c, d).

Compared to xenoliths from ocean-island or continental environments (Canary and Kerguelen Islands, Australia), the VVP xenoliths show more gently sloping arrays in the TiO<sub>2</sub> and CaO vs. MgO diagrams (Figs. 2b and d) and are characterized by a wide range of TiO<sub>2</sub> and CaO contents, with a variation of about 10 wt. % MgO. The positive array in the CaO vs. Al<sub>2</sub>O<sub>3</sub> plot (Fig. 2e), shown by both the VVP and French Massif Central, Germany, Hungary, Romania, Russia, Mongolia, China, Canadian Cordillera and Vulture xenoliths, indicates a mantle source depleted in a basaltic component after partial melting events. In particular, the more depleted xenoliths from the VVP plot towards the subduction-related xenoliths (Marianas, Papua New Guinea and the Philippines).

#### *Trace element composition*

Concentrations of compatible (Ni and Co) and incompatible (Rb, Nb, Zr, Hf, Y and Lu) elements of the VVP and worldwide xenoliths are plotted against MgO contents in Fig. 3 (literature sources for trace elements are the same as those for major elements). Among the compatible elements, Ni and Co display rough positive trends with MgO, due to the increase of residual olivine in the most Ni-Co-Mg-rich xenoliths, or to the increase of both Ni and Co contents in olivines (Figs. 3a and b). Among the incompatible trace elements, some of the High Field Strength Elements (HFSE) and HREE, such as Y, Lu, and, to a lesser extent, Hf, show rough negative correlations with MgO content (Figs. 3c, d, f). Zr, Nb and the Low Field Strength Elements (LFSE, e.g., Rb) are not correlated with MgO content (Figs. 3e, g, h). Three xenoliths, 55B, F56-7 and F56-17 display unusually high Rb, Th, Nb, Ta, Zr and Hf concentrations because of the interaction with the host material.

The slight negative correlations between HFSE and MgO depicted by the VVP and French Massif Central, Germany, Hungary, Romania, Russia, Mongolia, China, Canadian Cordillera and Vulture samples contrast with the flat trend defined by xenoliths from typical subduction zones (Marianas and Papua New Guinea) and with the almost vertical array formed by samples from Canary and Kerguelen Islands.

Most of the VVP samples show similar REE patterns (Fig. 4a, Table 3). The majority display variable enrichment in LREE, as indicated by their (Ce/Yb)<sub>n</sub> ratio varying from 0.46 to 8.22. The most LREE-enriched xenoliths [(Ce/Yb)<sub>n</sub> = 16.58–21.09] are those samples contaminated by the host basalt (55B, F56-7, and F56-17).

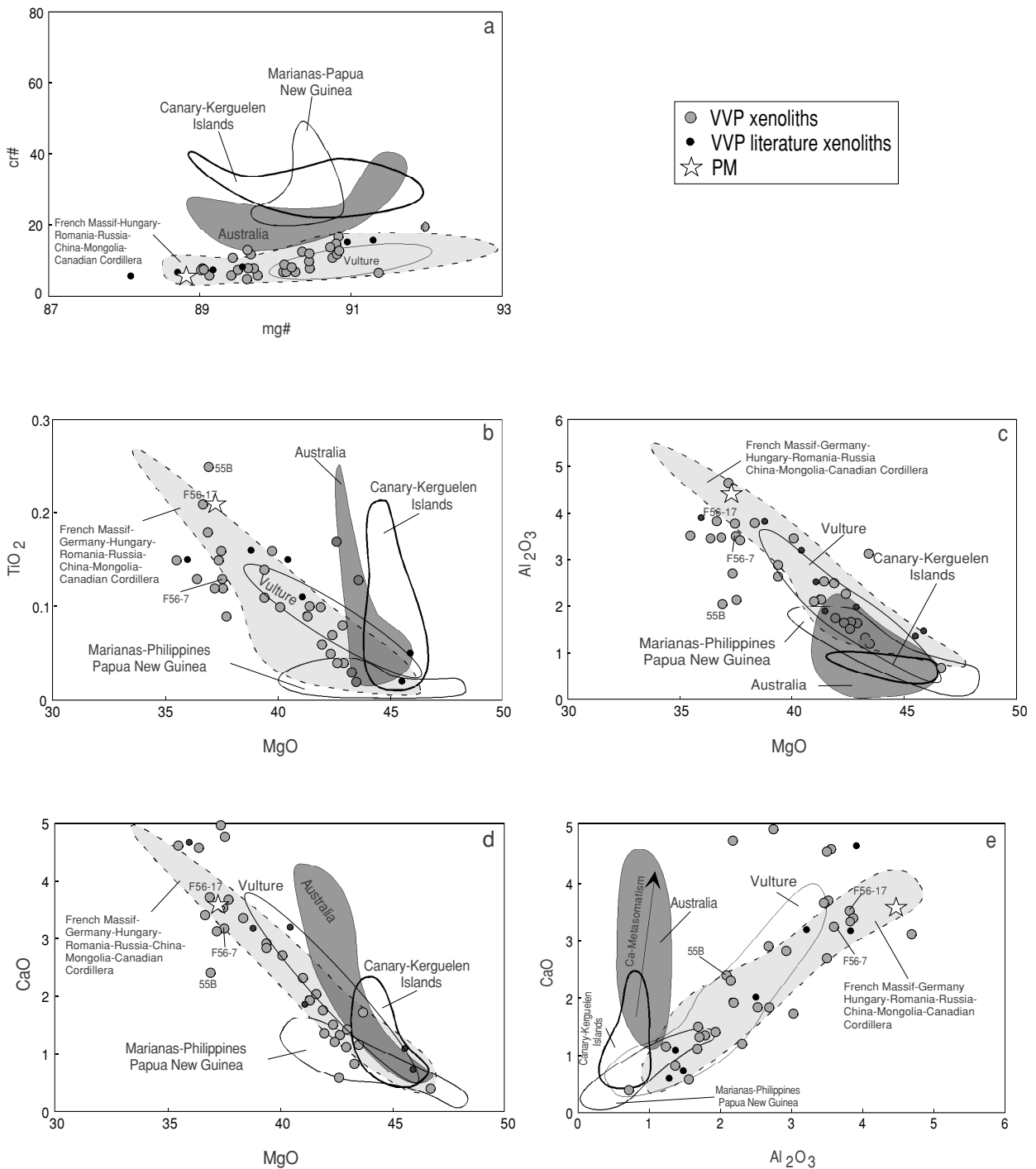


Fig. 2. Major element variations against MgO (wt. %), CaO vs. Al<sub>2</sub>O<sub>3</sub> and cr# vs. mg# covariations of the VVP xenoliths (this work, Table 3a; VVP literature data: Beccaluva et al., 2001), compared to the primordial mantle composition (McDonough, 1990) and world-wide mafic xenoliths. French Massif Central: Zangana et al., 1999; Lenoir et al., 2000; Germany: Hartmann and Wedepohl, 1990; Witt-Eickschen, 1993; Hungary: Downes et al., 1992; Romania: Vaselli et al., 1995; Russia: Ionov et al., 1995; China: Qi et al., 1995; Chen et al., 2001; Mongolia: Wiechert et al., 1997; Canadian Cordillera: Peslier et al., 2002; Vulture: Downes et al., 2002; Canary Islands: Wulff-Pedersen et al., 1996; Neumann et al., 2002; Kerguelen Islands: Grégoire et al., 1997; Australia: O'Reilly and Griffin, 1988; Yaxley et al., 1991; Foden et al., 2002; Marianas: Parkinson and Pearce, 1998; Papua New Guinea: Franz et al., 2002; Philippines: Maury et al., 1992. The array (Ca-metasomatism) is from Yaxley et al., 1991.

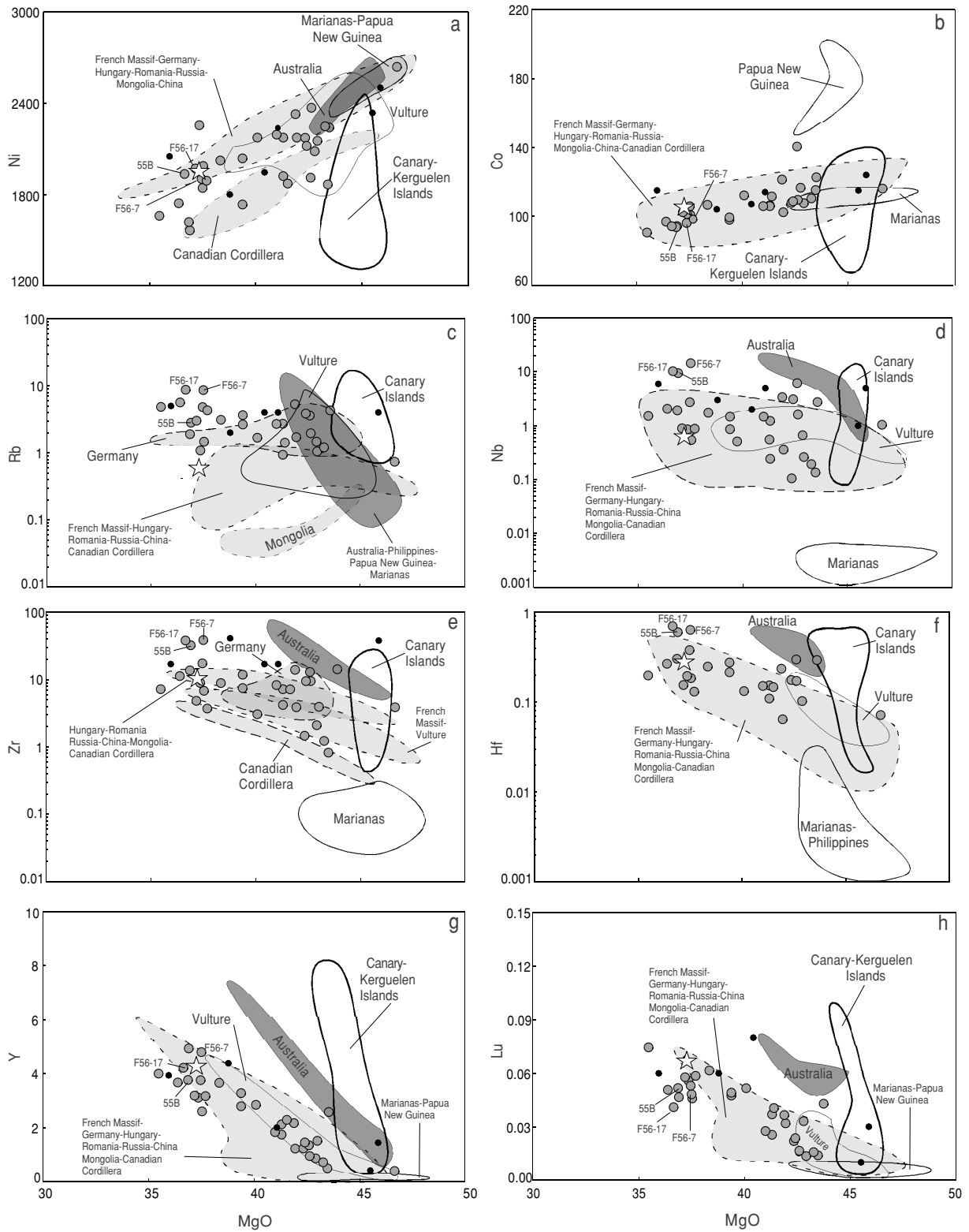


Fig. 3. Trace element abundances (ppm) vs. MgO content (wt.%) for the VVP xenoliths, compared to the primordial mantle composition (McDonough and Sun, 1995) and world-wide ultramafic xenoliths (references as in Fig. 2 plus Stosch and Lugmair, 1986, for Germany). Symbols are the same as in Fig. 2.

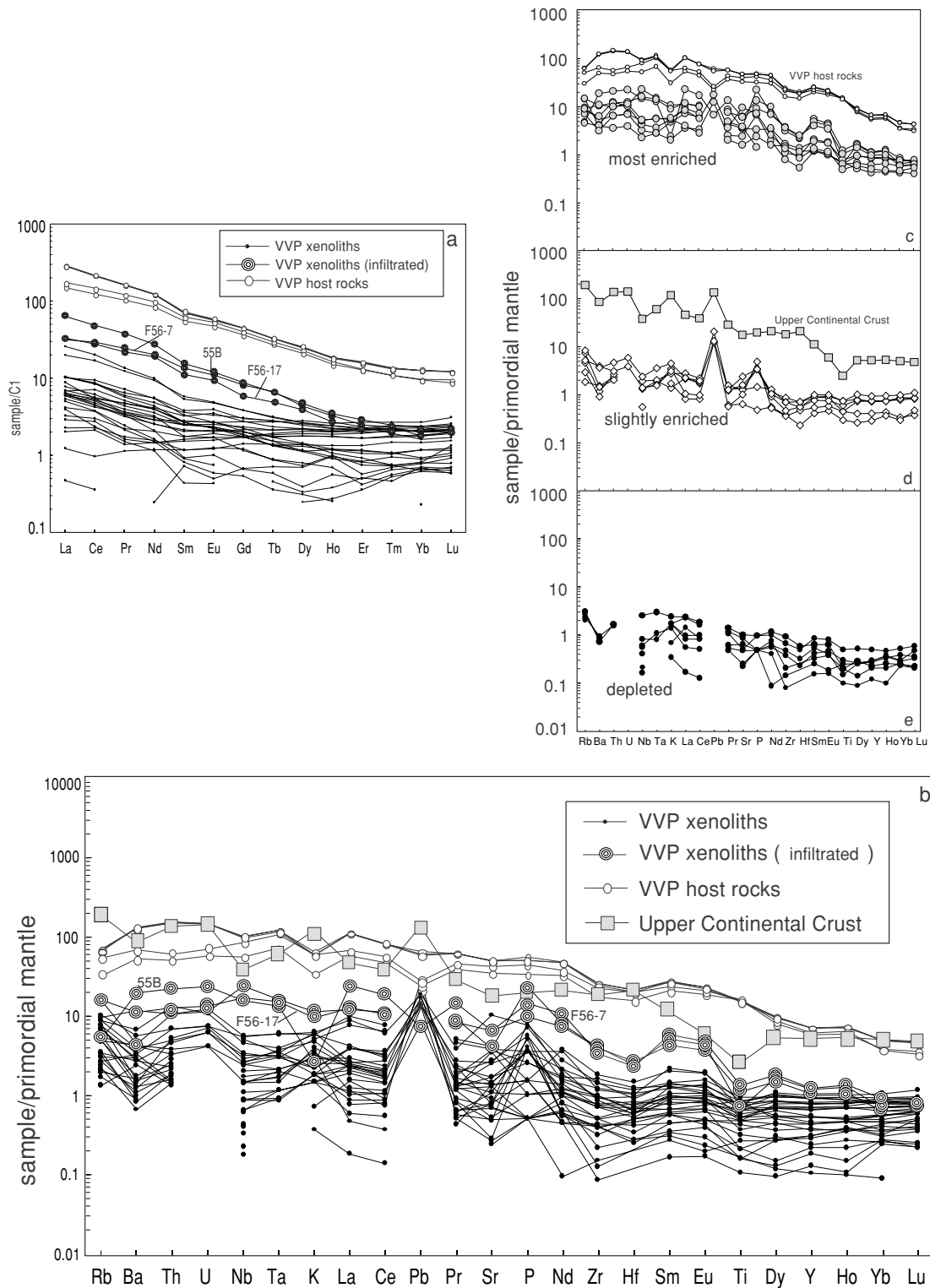


Fig. 4. a) CI-normalized (Sun and McDonough, 1989) REE patterns for the VVP bulk-rock xenoliths, compared to the VVP host lavas (this work, Table 3b). Primordial mantle-normalized (McDonough and Sun, 1995) trace element variation diagrams for bulk-rock peridotite xenoliths from the VVP (this work), compared to the VVP basanites and the upper continental crust (Taylor and McLennan, 1985): b) overview, c) the most incompatible element enriched samples, d) the slightly incompatible element enriched samples and e) the incompatible element depleted samples. In this figure, some VVP xenoliths characterized by incompatible element patterns with mixed signature (e.g., crust- and OIB-like trends) were left out for the sake of simplicity.

Primordial mantle-normalized bulk rock trace element abundances of the VVP xenoliths (Figs. 4b–e) show an enrichment of the most incompatible elements (from Rb to P) from one to twenty times the primordial mantle, with Pb peaks (enriched xenoliths; Fig. 4c) or troughs (below the detection limit for the most depleted xenoliths; Fig. 4e). The less incompatible elements (from Nd to Lu) have abundances similar to or lower than the primordial mantle (Fig. 4e). We note that:

1) the strongly contaminated xenoliths (55B, F56-7 and F56-17; Fig. 4c) are the most enriched in incompatible elements and display Nb-Ta peaks over the adjacent LREE, with K, Sr, Zr and Hf negative anomalies. Their patterns are actually similar to those of the VVP host basanites, which have a typical OIB signature, in spite of the lack of Rb negative anomalies in most of the samples (Fig. 4c, Table 3; Macera *et al.*, 2003). Other xenoliths display similar geochemical characteristics, also if relatively less enriched in incompatible elements, and not all showing K troughs, even if they do not display optical evidence of interaction with the host basanites;

2) most of the xenoliths which are slightly enriched in incompatible elements, apparently not contaminated by the host material, are characterized by peaks at Rb, Th, U and K, and troughs at Ba, Nb, Ta, Zr (Fig. 4d). Their patterns are analogous to that of sedimentary material, represented as the average upper continental crust (Taylor and McLennan, 1985) in Figs. 4b and d, thus significantly different with respect to OIB trends (here represented by the VVP host rocks). Nevertheless some of these xenoliths are characterized by Hf troughs;

3) the most depleted VVP xenoliths display slightly negative patterns from LILE to HFSE with Ba, Zr and Hf troughs, and lower enrichments in all the incompatible elements with respect to the enriched ones (Fig. 4e).

Interestingly, all xenoliths show Ti negative anomaly. As far as key incompatible element ratios, in the plot of La/Yb vs. Ti/Eu ratios (Fig. 5a) the VVP xenoliths define a trend parallel to the field including data from Russia, Mongolia, China and the Canadian Cordillera, thus showing similar La/Yb but higher Ti/Eu ratios. The majority of VVP xenoliths fall within the field of French Massif Central and Germany, but a few also plot within the fields of HIMU and pelagic sediments (Planck and Langmuir, 1998). The VVP xenoliths are characterized by significantly lower La/Yb ratios and higher Ti/Eu ratios with respect to both carbonatites (Nelson *et al.*, 1988; Klemme *et al.*, 1995) and carbonatite-metasomatized xenoliths (e.g., Australia, Yaxley *et al.*, 1991, 1998).

In the diagram of Tb/Yb ratio vs. Al<sub>2</sub>O<sub>3</sub> content (Figs. 5b and c; modified from Peslier *et al.*, 2002), several VVP xenoliths plot on the melting trend in the spinel stability field (Bodinier *et al.*, 1988), similarly to xenoliths from French Massif Central and Canadian Cordillera. Some

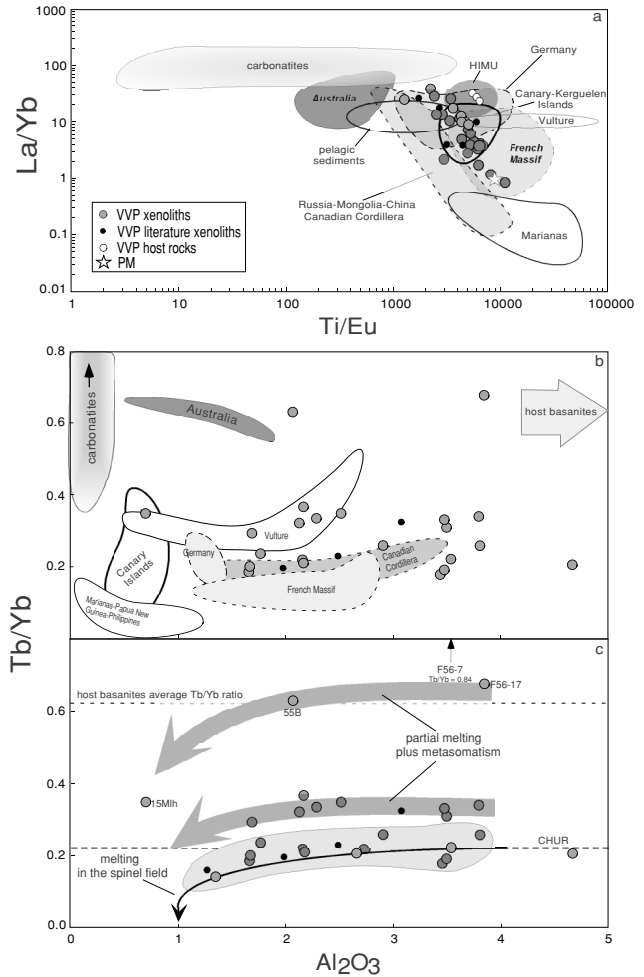


Fig. 5. (a) La/Yb vs. Ti/Eu, and (b and c) Tb/Yb ratio vs. Al<sub>2</sub>O<sub>3</sub> wt.% content (Peslier *et al.*, 2002; modified) for the VVP xenoliths and host basanites (white circles), compared to the VVP literature data (Beccaluva *et al.*, 2001) and other worldwide ultramafic xenoliths (references as in Fig. 2). In plot (c) some xenoliths from the VVP plot on a melting trend (black arrow) in the spinel stability field. High Tb/Yb ratios (>0.35) at similar Al<sub>2</sub>O<sub>3</sub> content (1–4% wt. ca) could be related to metasomatic processes in their mantle source (Peslier *et al.*, 2002, modified). Primordial mantle values from McDonough and Sun, 1995. Data for carbonatites are from Nelson *et al.* (1988) and Klemme *et al.* (1995). Fields for MOR-HIMU basalts are based on data from <http://petdb.ideo.columbia.edu/petdb/> and <http://georoc.mpch-mainz.gwdg.de/Start.asp>. Pelagic sediments are from Planck and Langmuir (1998). Host basanites average Tb/Yb ratio = 0.62. CHUR: Chondritic Uniform Reservoir.

VVP xenoliths display the same depletion trend but at higher Tb/Yb ratios (>0.35). This geochemical characteristic is also shown by xenoliths from Vulture. The host basanites are characterized by Tb/Yb ratios ranging from 0.59 to 0.72 and may have caused the highest Tb/Yb ra-

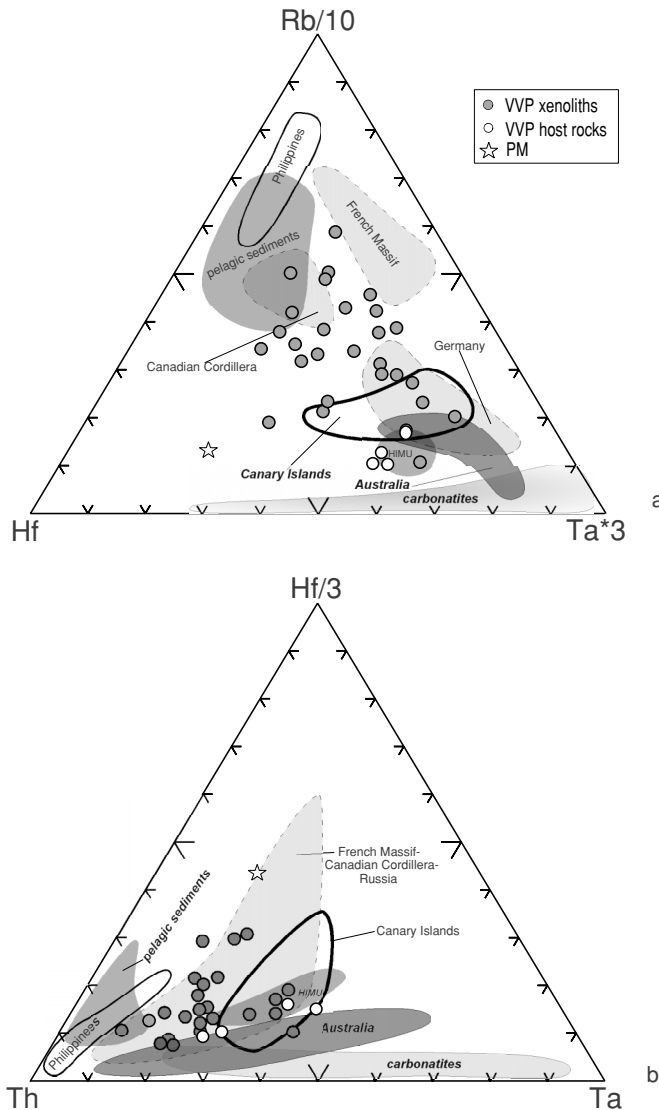


Fig. 6. (a) Hf-Rb/10-Ta\*3 diagram (Harris *et al.*, 1986; modified) and (b) Th-Hf/3-Ta diagram (Wood, 1980; modified) for the VVP and world-wide ultramafic xenoliths (references as in Fig. 2). For HIMU, pelagic sediments and carbonatites data references are as in Fig. 5. Primordial mantle values are from McDonough and Sun (1995).

tios recorded in the contaminated xenoliths (55B, F56-7, F56-17). Otherwise, we guess that the anomalously high Tb/Yb ratio of F56-B might be due to erroneous analysis, which leads to overestimation of Tb content (see Table 2b). Carbonatites display high Tb/Yb ratios as well (average Tb/Yb = 0.93; Nelson *et al.*, 1988; Klemme *et al.*, 1995) but at lower Al<sub>2</sub>O<sub>3</sub> content.

In both the Hf-Rb/10-Ta\*3 (Fig. 6a, modified from Harris *et al.*, 1986) and Th-Hf/3-Ta diagram (Fig. 6b; modified from Wood, 1980) the VVP xenoliths define a

roughly triangular field, the vertices of which are the HIMU-VVP host rocks field, the Primitive Mantle and the pelagic sediment field. Some of the VVP xenoliths fall within samples from French Massif Central, Germany, Russia and Canadian Cordillera (mostly in the Th-Hf/3-Ta diagram, Fig. 6b), whereas all plot significantly far from the field of carbonatites.

#### Isotopic composition

The Sr, Nd, Pb and O isotopic compositions of the VVP whole rock xenoliths are listed in Table 4. The <sup>87</sup>Sr/<sup>86</sup>Sr and <sup>143</sup>Nd/<sup>144</sup>Nd ratios range from 0.703031 to 0.704356 and from 0.512817 to 0.513085, respectively (Fig. 7a). The majority of the VVP ultramafic xenoliths display <sup>87</sup>Sr/<sup>86</sup>Sr (0.703031–0.703514) and <sup>143</sup>Nd/<sup>144</sup>Nd (0.512922–0.513085) ratios clustering in the area in which the fields of MORB and OIB overlap (insert in Fig. 7a; data from <http://petdb.Ideo.columbia.edu/petdb/>). In contrast, two xenoliths (25Mlh and 25Cmlh) show significantly more radiogenic Sr isotopic compositions (0.703940–0.704356), plotting outside the mantle-array (Fig. 7a), with <sup>87</sup>Sr/<sup>86</sup>Sr ratios respectively similar (25Mlh) and significantly higher (25Cmlh) than their host basanite (25MB). These xenoliths display a Sr isotopic signature that is often recorded in subduction-related basaltic andesites (Gill, 1981). Such a feature is commonly ascribed to low temperature alteration processes, e.g., related to interaction between oceanic floor and seawater occurring in altered oceanic crust (e.g., Davis *et al.*, 2003) or caused by late weathering.

With respect to Sr-Nd isotope data on worldwide xenoliths, the VVP samples show significant similarities with French Massif Central (Downes and Dupuy, 1987; Zangana *et al.*, 1997; Downes *et al.*, 2003), Germany (Hessian Depression; Kramm and Wedepohl, 1990) and the Pannonian Basin (Hungary and Romania: Downes *et al.*, 1992; Vaselli *et al.*, 1995; Rosenbaum *et al.*, 1997). The two VVP xenoliths characterized by the most radiogenic Sr isotopic compositions, 25Mlh and 25Cmlh, display Sr and Nd isotope ratios similar to those from Australia (McDonough and McCulloch, 1987; Griffin *et al.*, 1988), China (Song and Frey, 1989; Tatsumoto *et al.*, 1992) and Hungary (Rosenbaum *et al.*, 1997). Some VVP xenoliths with low Nd and Sr isotope ratios plot close to Canary Islands (Whitehouse and Neumann, 1995), within the field of VVP basalts (insert in Fig. 7a; data from Macera *et al.*, 2003). There are no similarities between xenoliths from the VVP and Japan, Philippines and the Kerguelen Islands.

The VVP ultramafic xenoliths show variable <sup>206</sup>Pb/<sup>204</sup>Pb (18.539–19.694), <sup>208</sup>Pb/<sup>204</sup>Pb (38.412–39.660) and <sup>207</sup>Pb/<sup>204</sup>Pb (15.608–15.664) isotopic ratios. In the <sup>207</sup>Pb/<sup>204</sup>Pb vs. <sup>206</sup>Pb/<sup>204</sup>Pb ratios plot (Fig. 7b), only two xenoliths (F56-16 and F56-17) fall on the mantle-array

Table 4. Sr, Nd, Pb and O isotope data for the VVP whole-rock xenoliths and host lavas. Analytical errors in the last decimal place.

Sample	Lithotype	Locality	$^{87}\text{Sr}/^{86}\text{Sr}$	$^{143}\text{Nd}/^{144}\text{Nd}$	$^{206}\text{Pb}/^{204}\text{Pb}$	$^{207}\text{Pb}/^{204}\text{Pb}$	$^{208}\text{Pb}/^{204}\text{Pb}$	$\delta^{18}\text{O}$
F56-3	sp-harzburgite	Adige Valley	0.703314	0.512994	19.104	15.636	38.841	6.6
F56-7	sp-harzburgite	Adige Valley	0.703458	0.512972	18.606	15.608	38.412	7.9
F56-8	sp-lherzolite	Adige Valley	0.703291	0.513085	19.094	15.642	38.909	7.1
			0.703300	0.513081				
F56-16	sp-lherzolite	Adige Valley	0.703251	0.512986	19.694	15.658	39.660	6.8
			0.703263	0.512984				
F56-17	sp-lherzolite	Adige Valley	0.703510	0.512967	19.524	15.638	39.316	7.3
36Mlh	sp-lherzolite	Lessini Mts.	0.703296	0.513025	18.609	15.610	38.486	8.3
			0.703303	0.513042				
28AMlh	sp-lherzolite	Lessini Mts.	0.703514	0.512984	18.539	15.619	38.442	6.6
25Mlh	sp-lherzolite	Lessini Mts.	0.703940	0.513044	18.721	15.641	38.774	6.7
					18.700	15.650	38.775	
25CMlh	sp-lherzolite	Lessini Mts.	0.704356	0.512990	18.808	15.651	38.893	11.2
					18.776	15.655	38.872	
					18.808	15.651	38.893	
SG3XEN	sp-lherzolite	Lessini Mts.	0.703320	0.512942	—	—	—	—
SG6XEN	sp-lherzolite	Lessini Mts.	0.703192	0.512817	—	—	—	—
6MB	basanite	Lessini Mts.	0.703778	0.512864	18.939	15.661	39.083	7.7
27MB	basanite	Lessini Mts.	0.703232	0.512953	19.400	15.625	39.127	7.5
28MB	basanite	Lessini Mts.	0.703247	0.512961	19.286	15.624	39.011	7.0
25MB	basanite	Lessini Mts.	0.703942	0.512833	18.900	15.667	39.081	8.2
			0.703940	0.512854				
56MB	basanite	Adige Valley	0.703465	0.512945	—	—	—	9.7

(hundreds of literature data, <http://georoc.mpch-mainz.gwdg.de/Start.asp>; <http://petdb.Ideo.columbia.edu/petdb/>), lining up with two of the VVP host basanites, whereas the other samples plot in the field of pelagic sediments (numerous literature data, courtesy B. Hanan, Fig. 7b). The Pb isotope characteristics described for the VVP xenoliths are recorded in peridotite samples that have been contaminated by sediment-enriched component (e.g., Ben Othman *et al.*, 1989; Weaver, 1991; Chauvel *et al.*, 1992). The Pb isotopic characteristics of the VVP xenoliths show similarities to those of xenoliths from Hungary and Romania (Rosenbaum *et al.*, 1997), especially from the western Pannonian Basin (Szentbékálka, Hungary). In the  $^{207}\text{Pb}/^{204}\text{Pb}$  vs.  $^{206}\text{Pb}/^{204}\text{Pb}$  ratios plot (Fig. 7b), the VVP xenoliths define a parallel trend but at higher  $^{207}\text{Pb}/^{204}\text{Pb}$  for similar  $^{206}\text{Pb}/^{204}\text{Pb}$  ratios to the sub-horizontal field of ultramafic xenoliths from Canary and Kerguelen Islands (Whitehouse and Neumann, 1995; Mattielli *et al.*, 1996; Fig. 7b). The Pb isotopic compositions and the  $^{87}\text{Sr}/^{86}\text{Sr}$  and  $^{143}\text{Nd}/^{144}\text{Nd}$  ratios of the VVP xenoliths are not correlated. Those samples that are characterized by the highest  $^{206}\text{Pb}/^{204}\text{Pb}$  ratios (e.g., F56-16) also show low  $^{87}\text{Sr}/^{86}\text{Sr}$  (Fig. 7c) and  $^{143}\text{Nd}/^{144}\text{Nd}$  ratios, displaying isotopic similarities to VVP OIB-HIMU-like basalts (Macera *et al.*, 2003). Moreover, the most Sr-radiogenic samples (25Mlh and 25CMlh) are characterized

by relatively low  $^{206}\text{Pb}/^{204}\text{Pb}$  ratios.

The oxygen isotopic compositions of the VVP bulk rock xenoliths range from 6.6 to 11.2‰ (Table 4). This  $\delta^{18}\text{O}$  range of variation is significantly higher than the normal mantle average ( $5.6 \pm 0.2\text{‰}$ ; Javoy, 1980), even in convergent margins ( $6.0 \pm 0.4\text{‰}$ ; Taylor, 1968, 1986; Muehlenbachs and Clayton, 1972; Magaritz *et al.*, 1978; Déruelle *et al.*, 1983; Ito and Stern, 1985; Pineau *et al.*, 1999), and exceeds that of the host basanites (7.0–9.7‰). High  $\delta^{18}\text{O}$  values, significantly deviating from the mantle average, are believed to be indicative of low-temperature processes occurred in rocks that were exposed to surface conditions (e.g., alteration of oceanic crust, residence in the upper crust, weathering) and/or related to recycling of sedimentary material in their mantle sources (e.g., Taylor and Sheppard, 1986). Oxygen isotopic compositions of the VVP xenoliths are not clearly correlated with  $^{87}\text{Sr}/^{86}\text{Sr}$  ratios (Fig. 7d). In particular, as with the Sr-Nd isotope relationship, the VVP xenoliths cluster in a relatively restricted range of Sr isotopic composition (0.703031–0.703514) and  $\delta^{18}\text{O}$  (6.6–8.3‰), although the sample with the highest  $^{87}\text{Sr}/^{86}\text{Sr}$  ratio (25CMlh) is characterized by the highest  $\delta^{18}\text{O}$  value (Fig. 7d). In contrast, there is a negative correlation between silica contents and oxygen isotope compositions, for which the most Si-rich xenoliths show the lowest  $\delta^{18}\text{O}$  values (Fig. 7e).

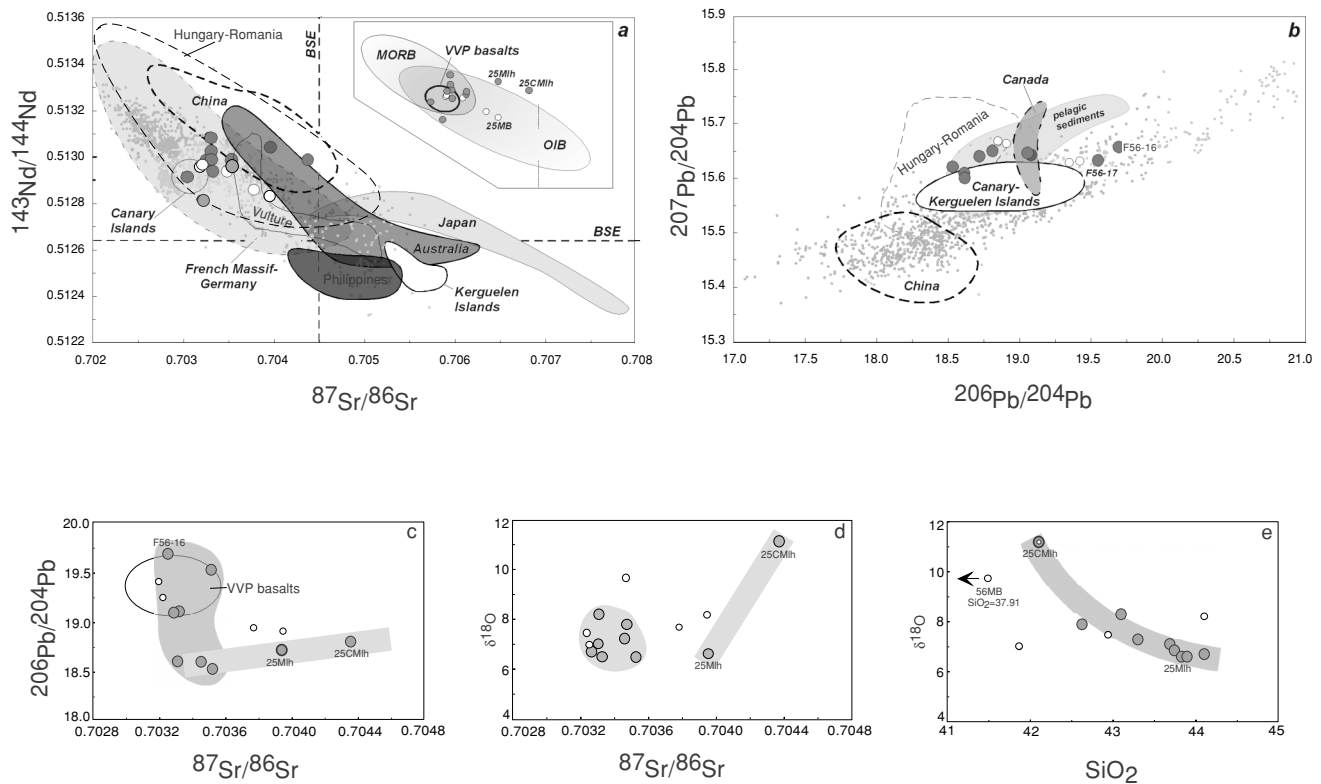


Fig. 7. (a)  $^{143}\text{Nd}/^{144}\text{Nd}$  vs.  $^{87}\text{Sr}/^{86}\text{Sr}$  ratios for ultramafic xenoliths and host lavas from the Veneto Volcanic Province (this work), compared to various world-wide ultramafic xenoliths (French Massif Central: Downes and Dupuy, 1987; Zangana et al., 1997; Downes et al., 2003; Germany-Hessian Depression: Kramm and Wedepohl, 1990; Hungary and Romania: Downes et al., 1992; Vaselli et al., 1995; Rosenbaum et al., 1997; Vulture: Downes et al., 2002; Australia: McDonough and McCulloch, 1987; Griffin et al., 1988; China: Song and Frey, 1989; Tatsumoto et al., 1992; Canary Islands: Whitehouse and Neumann, 1995; Kerguelen Islands: Mattielli et al., 1996; Philippines: Vidal et al., 1989; Maury et al., 1992; Japan: Ikeda et al., 2001). The mantle array data is from (<http://petdb.Ideo.columbia.edu/petdb/>). The insert shows the position of OIB and MORB fields with respect to the VVP xenoliths and their host rocks (this work), and VVP basalts from literature (Macera et al., 2003). BSE: Bulk Silicate Earth. (b)  $^{207}\text{Pb}/^{204}\text{Pb}$  vs.  $^{206}\text{Pb}/^{204}\text{Pb}$  ratios plot for ultramafic xenoliths and host basanites from the Veneto Volcanic Province (this work), compared to mafic xenoliths from Canary and Kerguelen Islands (Whitehouse and Neumann, 1995; Mattielli et al., 1996), Hungary and Romania (Rosenbaum et al., 1997), China (Tatsumoto et al., 1992) and Canada (Yukon; Carignan et al., 1996). The field of pelagic sediments is contoured from numerous literature data (courtesy B. Hanan); the mantle-array data (small grey filled circles) are from <http://petdb.Ideo.columbia.edu/petdb/>. (c)  $^{206}\text{Pb}/^{204}\text{Pb}$  vs.  $^{87}\text{Sr}/^{86}\text{Sr}$  ratios, (d)  $\delta^{18}\text{O}$  vs.  $^{87}\text{Sr}/^{86}\text{Sr}$  ratios, and (e)  $\delta^{18}\text{O}$  vs.  $\text{SiO}_2$  wt.% diagrams for ultramafic xenoliths and host basanites from the Veneto Volcanic Province (this work). VVP basalts are from Macera et al., 2003. Symbols are the same as in Fig. 5.

## DISCUSSION

The goal of this work is to investigate eventual marks of mantle processes that have affected the VVP subcontinental lithosphere. In this study we deal with whole-rock and mineral geochemistry of the VVP xenoliths, being aware that whole-rock Sr, Pb and O isotope analyses could lead to erroneous conclusions, since cryptic but pervasive alteration is sometimes recorded in such material. Sr, Nd (Hf) and Pb isotope data on acid-washed clinopyroxenes is considered to be the most reliable technique for the identification of isotopic mantle signature

since the Seventies. Otherwise, only a few, not representative mantle xenoliths from the Adige Valley are suitable for clinopyroxene separation, whereas the presence of spongy and/or secondary clinopyroxenes and the small size of the Lessini Mts. xenoliths make prohibitive this approach. We cannot presumptively exclude cryptic alteration for the remnant xenoliths of this data set. Nevertheless, we noted that Th, Nb, Ta, Zr and Hf enrichments are strictly related to OIB modification, but actually characterize only a few VVP xenoliths. Moreover, we suppose that weathering should induce mobile element enrichments, while contamination with  $^{18}\text{O}$  rich crust

during intracrustal differentiation should cause positive correlations between  $\delta^{18}\text{O}$  and  $\text{SiO}_2$  contents and/or  $^{87}\text{Sr}/^{86}\text{Sr}$  ratios (Taylor and Turi, 1976). The fact that the VVP xenoliths (i) do not show petrographical evidence of surface alteration, (ii) show negative correlations between their silica contents and oxygen isotope data, (iii) also displaying  $\delta^{18}\text{O}$  values that, when higher than 7‰, are higher than those of the host basanites which incorporate them, allows to assume that the following data discussion is a suitable approach to face the origin of the VVP subcontinental mantle heterogeneity.

Bulk-rock major element geochemistry indicates that nearly all the xenoliths, regardless of their texture, are slightly to strongly depleted in a basaltic component relative to the primordial mantle (Fig. 2). The protogranular textures of the Adige Valley samples and their low equilibration temperature suggest that after the partial melting event the xenoliths equilibrated and cooled under spinel-facies conditions. The samples from the Lessini Mts. retain reaction textures such as spongy clinopyroxenes with tiny inclusions of glass. The origin of spongy textures in clinopyroxene may be explained by the breakdown of the mineral during high-temperature transport of the xenoliths to the surface in their host magmas (see also Yaxley and Kamenetsky, 1999). However, spongy textures may also develop in response of interactions between the mantle mineral assemblage and transient metasomatic liquids and/or fluids (Chazot *et al.*, 1996, Coltorti *et al.*, 2000, Carpenter *et al.*, 2002). Therefore, we cannot exclude that the spongy textures of clinopyroxene may be the result of reactions between clinopyroxenes and a metasomatic agent.

Mineral chemistry variations of clinopyroxenes and spinels cannot be explained with the partial melting process supported by the bulk-rock major element data. An inspection of Tables 2c and 2d reveals that there is no positive correlation between cr# and mg# in spinels. In addition, no positive correlation is observed between the  $\text{Al}_2\text{O}_3$  contents of spinels and coexisting clinopyroxenes. As already emphasized by Morten *et al.* (1989) for spinels from the S. Giovanni Ilarione (Lessini Mts.) site, the deviation from the partial melting trend may derive from solid-liquid reactions (e.g., reactions between the mantle-parageneses and ephemeral metasomatic liquids). Given that the depleted and fertile character of the VVP xenoliths is irrespective of texture, we may infer that metasomatic events occurred early in the history of the Veneto lithosphere and in any case prior to the entrapment of the xenoliths in the host magmas.

Metasomatic agents in the source of the VVP xenoliths have been mostly related to OIB melts, penetrating into the shallow mantle by upwelling to the surface (Siena and Coltorti, 1989; Coltorti *et al.*, 2000; Beccaluva *et al.*, 2001; Bonadiman *et al.*, 2001; Morten *et al.*, 2002; Morten

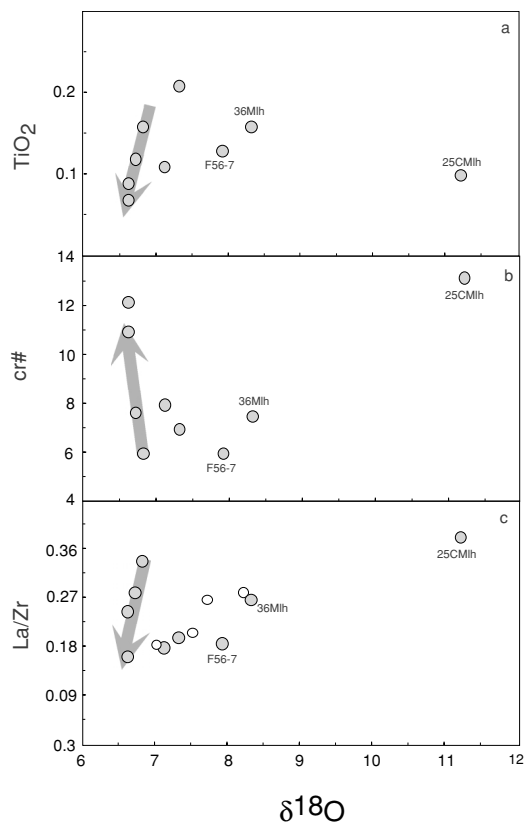


Fig. 8.  $\text{TiO}_2$  wt.% contents (a), cr# values (b) and La/Zr ratio (c) vs.  $\delta^{18}\text{O}$  values for the VVP xenoliths and host basanites. Xenoliths with  $\delta^{18}\text{O} \leq 7.0\text{‰}$  plot on an increasing melting trend. Xenoliths with  $\delta^{18}\text{O} > 7.0\text{‰}$  could be related to fluxed batch or fractional melting driven by different slab-derived components.

*et al.*, 2004). In particular, Beccaluva *et al.* (2001), following the approach of Coltorti *et al.* (1999), carried out major and trace element mass balance calculations to identify a possible metasomatic agent for the VVP xenoliths. The composition of the hypothetical melt shows similarities to both the Late-Cretaceous Na-alkaline lamprophyres and the VVP alkaline basic lavas. Evidence of reaction in orthopyroxenes, clinopyroxene and spinel, together with consumption of olivine in the primary assemblage, could be due to the addition of 1–6% of the calculated Na-alkaline basic melt.

Nevertheless, the VVP xenoliths do not show OIB-like uniform patterns in multi-element spiderdiagrams and are characterized by a large spread in incompatible trace element ratios (e.g., Figs. 4, 5, 8). Similar characteristics have been highlighted in ultramafic xenoliths from extensional or extensional-subduction related environment, e.g., French Massif Central, Germany and Vulture (Downes, 2001). We observed that:

- 1) Some of the most incompatible element-enriched

xenoliths display geochemical features similar to those of the VVP host basanites, e.g., significant Nb-Ta positive anomalies, K troughs, comparable trace element ratios (e.g., La/Yb, Rb/Nb, Th/Yb, Tb/Yb, Sr/Yb), and Sr, Nd, Pb and O isotope compositions. Such geochemical characteristics are clearly related to physical interaction with the host basanites. Otherwise, the presence of xenoliths characterized by a HIMU-OIB (e.g., VVP-basanites) signature (Figs. 5a and 6b), not showing apparent petrographic contamination by the host basanites, may still be the result of OIB-related cryptic metasomatism. Actually, in ultramafic xenoliths MREE-enrichment with respect to HREE (e.g., high Tb/Yb ratios; Figs. 5b and c) and, more generally, the variable (from depleted to enriched) contents in highly incompatible trace elements (Nb, Ta, Rb, Ba and U), might be explained as the chromatographic effect induced by plume-derived melts percolating through a depleted peridotite and affecting incompatible elements and REE in order of increasing partition coefficient (up to MREE; Bodinier *et al.*, 1990; Takazawa *et al.*, 1992; Bedini *et al.*, 1997).

2) Conversely, the slightly incompatible element-enriched xenoliths show multi-element spectra (Ba-Nb-Ta negative anomalies and Rb peaks) that resemble those of sediments (Figs. 4b and d) and are discordant with respect to the HIMU-OIB modified patterns. They are also characterized by high LFSE/HFSE ratios, e.g., Rb/Nb, Ba/Zr, relatively radiogenic Sr isotopic compositions, high  $\delta^{18}\text{O}$  values and low  $^{206}\text{Pb}/^{204}\text{Pb}$  ratios. Since surface alteration does not seem to have significantly affected the VVP xenoliths, these peculiarities might reflect processes occurred in their mantle source, likely pointing to recycling of a slab-derived component with a significant pelagic sediment signature (Hawkesworth *et al.*, 1994; Elliott *et al.*, 1997; Kogiso *et al.*, 1997; Green and Adam, 2003). It might imply that the VVP subcontinental mantle was also affected by metasomatic agents released by a subducting plate, e.g., the European slab (subduction-related metasomatism) (Rosenbaum *et al.*, 1997; Downes, 2001; Downes *et al.*, 2002). Overlapping of metasomatic processes, e.g., OIB- and slab-type, is in agreement with both the lack of Rb troughs even in samples showing geochemical patterns comparable to HIMU-OIB (VVP lavas) and the occurrence of Ti negative anomalies within the whole suite of xenoliths.

3) Finally, the most depleted VVP xenoliths show geochemical features (e.g., trace element contents, Figs. 3 and 4e) that suggest they may derive from a mantle source which did not experience intense metasomatism, while reflecting great extent of depletion in a basaltic component.

In favor of the above hypotheses are the relationships between  $\text{TiO}_2$  (Fig. 8a),  $\text{Na}_2\text{O}$  (not shown),  $\text{cr}\#$  (Fig. 8b) values, LREE/HFSE ratios (e.g., La/Zr, Fig. 8c) and oxy-

gen (strontium) isotopic compositions. Mantle xenoliths characterized by low  $\text{TiO}_2$  and  $\text{Na}_2\text{O}$  contents and high  $\text{cr}\#$  values are interpreted as representative of residual mantle after variable degrees of partial melting (Figs. 8a and b). Depletion events may produce slightly positive correlations between  $\delta^{18}\text{O}$  and  $\text{Na}_2\text{O}$  or  $\text{TiO}_2$  contents, and negative correlations between  $\delta^{18}\text{O}$  and  $\text{cr}\#$ , inducing about 1‰ variation in  $\delta^{18}\text{O}$  because of the oxygen isotopes fractionation among coexisting minerals and melts (Weis *et al.*, 1987; Chiba *et al.*, 1989; Matthey *et al.*, 1994; Zheng, 1993). The group of VVP xenoliths that are characterized by  $\delta^{18}\text{O} \leq 7.0\text{‰}$ , and for which the whole range of oxygen isotope variation is less than 1‰, thus plotting on almost vertical trends in the plots of  $\delta^{18}\text{O}$  and  $\text{Na}_2\text{O}$  or  $\text{TiO}_2$  contents, can be explained by simple Rayleigh oxygen isotope fractionation during partial melting (Figs. 8a and b). This hypothesis appears to be supported by the distribution of this group of xenoliths in analogous sharply sloping trends in diagrams of LREE/HFSE ratios vs.  $\delta^{18}\text{O}$  values (e.g., Fig. 8c).

It was also proposed that aqueous fluids (up to about 2%) released from subducting plates can depress the mantle solidus and enhance partial melting on the overriding mantle wedge. This causes a sharp increase of the  $\text{cr}\#$  values, and a decrease of  $\text{TiO}_2$  ( $\text{Na}_2\text{O}$ ) and volatile elements contents, while  $\delta^{18}\text{O}$  values only slight increases in the residual peridotites (Eiler *et al.*, 2000). Conversely, samples F56-7, 36Mlh and 25CMLh, showing the highest  $\delta^{18}\text{O}$  values at relatively low  $\text{Na}_2\text{O}$  and  $\text{TiO}_2$  contents, might reflect the result of different processes able to add  $^{18}\text{O}$  without affecting the fusible components. Fluxed batch or fractional melting driven by slab-derived silicate melts (not fluids) could account for sharp rise in  $\delta^{18}\text{O}$  at nearly constant  $\text{TiO}_2$  ( $\text{Na}_2\text{O}$ ) and  $\text{cr}\#$  values (Eiler *et al.*, 2000), as observed for samples F56-7 and 36MLh (Fig. 8c). Otherwise, in diagrams of LILE/HFSE or LREE/HFSE ratios vs.  $\delta^{18}\text{O}$  (or  $^{87}\text{Sr}/^{86}\text{Sr}$ ) these two xenoliths fall on the most gently sloping array along with their host basanites, possibly reflecting variably interaction processes with the latter. Conversely, sample 25CMLh, which is the only VVP xenolith that shows both very high Sr and oxygen isotope compositions (Figs. 7 and 8), might represent a portion of the VVP subcontinental mantle metasomatized by slab-derived melts and fluids, as its pyrometamorphic texture may suggest, or it may more simply reflect hidden weathering processes.

Carbonatite-related metasomatism has been suggested among the possible metasomatic components to explain the geochemical peculiarities of within-plate xenoliths and volcanics (e.g., Australia; Yaxley *et al.*, 1991, 1998). In the case of the VVP xenoliths, carbonatite-related metasomatism does not seem to have significantly affected the lithospheric mantle beneath the VVP. Carbonatites are characterized by depletion of Ti, Zr, Hf, Rb, Sr and Nb

Table 5a. Major element and modal weight compositions for reactants (possible primary assemblages, average minerals for the VVP xenoliths and different metasomatizing liquids: 701 Ssand, Planck and Langmuir, 1998; post Arch. Terrains average, Rudnick and Fountain, 1995) and products obtained by mass balanced reactions. Theoretical compositions are compared to those of representative VVP xenoliths showing geochemical features similar to sedimentary material (see Fig. 4d).

	Reactants									
	Whole-rock				Mineral phases				Metasomatic liquids	
	25AMlh	36Mlh	SG3	MA7	cpx	opx	sp	ol	701 Ssand	post arch Terr
SiO <sub>2</sub>	43.37	43.09	45.12	44.94	54	53	—	41	71.30	49.7
TiO <sub>2</sub>	0.1	0.16	0.16	0.13	1	—	—	—	0.46	0.95
Al <sub>2</sub> O <sub>3</sub>	3.47	3.8	3.21	3.32	3	6	58	—	9.56	14.5
FeO*	9.31	9.37	9.25	8.39	8	6	13	10	4.06	11.3
MnO	0.13	0.13	0.13	0.13	—	—	—	—	0.06	0.19
MgO	40.03	38.29	37.37	39.7	16	31	19	49	1.73	8.53
CaO	2.72	3.37	4.47	3	20	2	—	—	1.06	9.72
Na <sub>2</sub> O	0.16	0.21	0.22	0.27	1	—	—	—	2.58	2.56
K <sub>2</sub> O	0	0.06	0.09	0.09	—	—	—	—	1.97	0.7
P <sub>2</sub> O <sub>5</sub>	0.08	0.16	0.03	0.03	—	—	—	—	0.10	0.19

	Significant mass balance results										Metasomatized VVP xenoliths				
	25AMlh + post arch Terr					36Mlh + 701 Ssand					Whole-rocks				
	4%	5%	6%	7%	8%	1%	2%	3%	4%	5%	6Mlh	25Mlh	25BMlh	F56-2A	F56-10
SiO <sub>2</sub>	43.92	44.0	44.0	44.1	44.2	44.0	44.3	44.6	44.9	45.2	44.94	44.11	45.33	42.5	43.38
TiO <sub>2</sub>	0.1	0.2	0.2	0.2	0.2	0.2	0.2	0.2	0.2	0.2	0.09	0.12	0.15	0.15	0.06
Al <sub>2</sub> O <sub>3</sub>	4.0	4.1	4.2	4.3	4.4	3.9	4.0	4.0	4.1	4.1	3.43	4.66	3.53	2.72	1.76
FeO*	9.4	9.4	9.4	9.4	9.4	9.5	9.4	9.4	9.3	9.3	8.56	9.05	8.12	8	7.901
MnO	0.1	0.1	0.1	0.1	0.1	0.1	0.1	0.1	0.1	0.1	0.13	0.13	0.12	0.13	0.13
MgO	39.1	38.8	38.5	38.3	38.0	38.5	38.1	37.8	37.5	37.2	37.64	37.12	35.42	37.3	41.89
CaO	3.0	3.1	3.1	3.2	3.2	3.4	3.4	3.4	3.3	3.3	3.69	3.14	4.63	4.98	1.37
Na <sub>2</sub> O	0.2	0.3	0.3	0.3	0.3	0.2	0.3	0.3	0.3	0.3	0.26	0.29	0.37	0.05	0
K <sub>2</sub> O	0.0	0.0	0.0	0.1	0.1	0.1	0.1	0.1	0.1	0.2	0.1	0.09	0.13	0.04	0.05
P <sub>2</sub> O <sub>5</sub>	0.1	0.1	0.1	0.1	0.1	0.2	0.2	0.2	0.2	0.2	0.1	0.07	0.07	0.07	0.01
	Modal compositions														
ol	60.31	59.17	58.06	56.96	55.89	59.2	57.2	55.2	53.3	51.4	54.3	51.9	47.2	61.7	68.0
opx	23.21	23.88	24.54	25.19	25.83	21.8	24.2	26.5	28.8	31.0	27.6	29.9	29.3	10.3	27.4
cpx	12.97	13.28	13.59	13.89	14.18	15.3	15.0	14.8	14.5	14.3	15.2	13.1	19.5	22.3	13.7
sp	3.61	3.72	3.83	3.94	4.05	3.5	3.4	3.3	3.1	3.0	1.9	4.1	1.6	2.1	0.3

	SG3 + 701 Ssand					MA7 + post arch Terr					Whole-rocks				
	1%	2%	3%	4%	5%	3%	4%	5%	6%	7%	6Mlh	25Mlh	25BMlh	F56-2A	F56-10
	SiO <sub>2</sub>	45.4	45.7	46.0	46.2	46.5	45.1	45.2	45.2	45.3	45.3	44.94	44.11	45.33	42.5
TiO <sub>2</sub>	0.2	0.2	0.2	0.2	0.2	0.2	0.2	0.2	0.2	0.2	0.09	0.12	0.15	0.15	0.06
Al <sub>2</sub> O <sub>3</sub>	3.3	3.3	3.4	3.5	3.5	3.7	3.8	3.9	4.0	4.1	3.43	4.66	3.53	2.72	1.76
FeO*	9.2	9.2	9.1	9.1	9.0	8.4	8.4	8.4	8.5	8.5	8.56	9.05	8.12	8	7.901
MnO	0.1	0.1	0.1	0.1	0.1	0.1	0.1	0.1	0.1	0.1	0.13	0.13	0.12	0.13	0.13
MgO	37.0	36.7	36.4	36.1	35.8	38.8	38.5	38.3	38.0	37.7	37.64	37.12	35.42	37.3	41.89
CaO	4.4	4.4	4.4	4.3	4.3	3.2	3.2	3.3	3.4	3.4	3.69	3.14	4.63	4.98	1.37
Na <sub>2</sub> O	0.2	0.3	0.3	0.3	0.3	0.3	0.4	0.4	0.4	0.4	0.26	0.29	0.37	0.05	0
K <sub>2</sub> O	0.1	0.1	0.1	0.2	0.2	0.1	0.1	0.1	0.1	0.1	0.1	0.09	0.13	0.04	0.05
P <sub>2</sub> O <sub>5</sub>	0.0	0.0	0.0	0.0	0.0	0.0	0.0	0.0	0.0	0.0	0.1	0.07	0.07	0.07	0.01
	Modal compositions														
ol	56.4	54.4	52.4	50.5	48.7	56.2	55.1	54.0	52.9	51.9	54.3	51.9	47.2	61.7	68.0
opx	20.7	23.1	25.4	27.7	29.9	29.7	30.3	30.9	31.5	32.0	27.6	29.9	29.3	10.3	27.4
cpx	20.7	20.3	20.0	19.7	19.4	12.0	12.3	12.6	12.9	13.3	15.2	13.1	19.5	22.3	13.7
sp	2.1	2.0	1.9	1.7	1.6	2.3	2.4	2.5	2.7	2.8	1.9	4.1	1.6	2.1	0.3

Table 5b. Modeled Sr isotope compositions and key trace element ratios for increasing percentages of sedimentary-rich liquid in the VVP subcontinental source. Least-squared regression is always below 0.5 and generally around 0.2–0.3. 25AMlh and 36MLh are from this work, SG3 and 6MLh are from Beccaluva *et al.* (2001). See text for further details and refer to Fig. 9 for a graphical representation of these results.

	Reactants		Added fraction of metasomatizing liquid (%)					Metasomatized VVP xenoliths				
	36Mlh	701Ssand	0.01	0.02	0.03	0.04	0.05	25Mlh	F56-2A	F56-10	6Mlh	25BMlh
<sup>87</sup> Sr/ <sup>86</sup> Sr	0.703296	0.709189	0.703730	0.704112	0.704450	0.704752	0.705023	0.703940	—	—	—	—
Nb/K	0.0036	0.0003	0.0028	0.0023	0.0019	0.0017	0.0015	0.0012	0.0027	0.0009	0.0011	0.0015
Ba/Th	22	212	43	60	74	86	97	103	54.3	—	59.4	64.8
Hf/Sm	0.47	1.01	0.49	0.52	0.54	0.56	0.57	0.50	0.54	0.38	0.60	0.49

	Reactants		Added fraction of metasomatizing liquid (%)					Metasomatized VVP xenoliths				
	25AMlh	post arch Terr	0.06	0.07	0.08	0.09	0.1	25Mlh	F56-2A	F56-10	6Mlh	25BMlh
<sup>87</sup> Sr/ <sup>86</sup> Sr	0.70351	—	—	—	—	—	—	0.703940	—	—	—	—
Nb/K	0.0023	0.0013	0.0018	0.0018	0.0018	0.0017	0.0017	0.0012	0.0027	0.0009	0.0011	0.0015
Ba/Th	98	52	68	67	65	64	63	103	54	—	59	65
Hf/Sm	0.44	0.58	0.48	0.48	0.48	0.49	0.49	0.50	0.54	0.38	0.60	0.49

relative to the REE, and high LREE-MREE/HREE ratio (Nelson *et al.*, 1988; Hauri *et al.*, 1993; Downes *et al.*, 2002). Trace element contents (Fig. 6) and ratios (Fig. 5) of the VVP xenoliths are not consistent with such a possible metasomatic agent. Moreover, the VVP xenoliths are not characterized by carbonatite signatures such as high Nb/La and very high Zr/Hf and Ca/Al ratios, or by the presence of Ca-LREE-rich phases such as apatite (e.g., Rudnick *et al.*, 1993).

*Modeling slab-derived metasomatic processes* In order to test our hypothesis and better constrain the geochemical signature of the metasomatizing slab-derived agent, we performed mass balance calculations to account for the geochemical compositions of the VVP xenoliths that are slightly enriched in incompatible elements (Fig. 4d), e.g., those showing trace element features similar to the upper continental crust and/or pelagic sediments. Among our sample collection we could not absolutely recognize a possible primary (undepleted and unmetasomatized) mantle assemblage, since overlapping of different metasomatic processes and various extents of depletion appears to have variably affected the VVP mantle lithosphere. Thus we selected four suitable xenoliths from both this collection (25AMlh, undepleted, and 36MLh, slightly enriched) and literature data (SG3, undepleted and unmetasomatized, and MA7, slightly depleted; Beccaluva *et al.*, 2001), supposing they reacted with two diverse metasomatic agents, which percolated and metasomatized the VVP mantle lithosphere (Table 5). In the calculations, the assumed compositions of the metasomatic agents are those of the 701 Ssand (Planck and Langmuir, 1998) and the post Archean Terrains average (Rudnick and Fountain, 1995), the choice of which derives from their different features in terms of major and trace element chemistry, reflecting possible components characterizing a hypothetical subducted crust.

In reactions such those in which a primary assemblage and a metasomatic agent interact to give a secondary assemblage (e.g., the metasomatized composition), the weight fraction  $F$  of each element  $i$  in the secondary assemblage can be assumed as:

$$F_i = \frac{a_{i,M}(P_M) + \sum_{i \neq M} a_{i,j}(P_j)}{100 + P_M}$$

where  $a_{i,M}$  is the weight fraction of element  $i$  in the metasomatizing liquid;  $P_M$  is the weight percent of the metasomatizing liquid;  $a_{i,j}$  is the weight fraction of the element  $i$  in the phase  $j$  of the primary assemblage;  $P_j$  is the weight percent of the phase  $j$  in the starting assemblage. The new composition (the metasomatized assemblage) is then recast in terms of the same compositions of

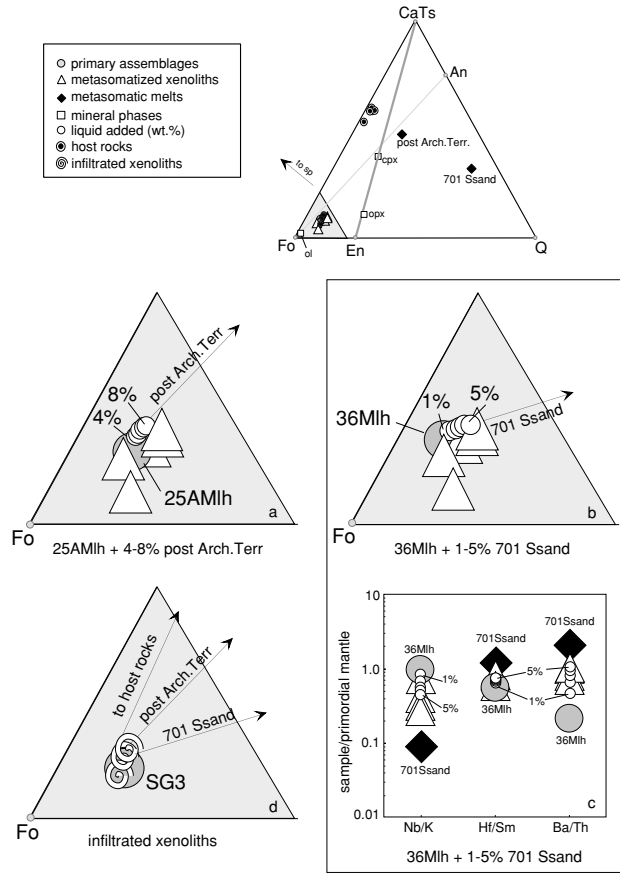


Fig. 9. Projection onto the forsterite (Fo)-Ca-Tschermak (CaTs)-Quartz (Qz) plane of the Qz-Fo-CaTs-Di (diopside) system of major element compositions of some hypothetical primary assemblages, sedimentary metasomatic liquids, metasomatized assemblages and mass balanced results for metasomatic reactions for the VVP xenoliths (refer to Table 5a), after recast of analyses in terms of CMAS components (O'Hara, 1968). Matrix to obtain a projection in the system Q-Ol-CaTs-Di in terms of CMAS components:  $C = [\text{mol. prop.} (\text{CaO} - 3.33\text{P}_2\text{O}_5 + 2\text{Na}_2\text{O} + 2\text{K}_2\text{O})] * 56.08$ ;  $M = [\text{mol. prop.} (\text{FeO} + \text{MnO} + \text{NiO} + \text{MgO} - \text{TiO}_2)] * 40.31$ ;  $A = [\text{mol. prop.} (\text{Al}_2\text{O}_3 + \text{Cr}_2\text{O}_3 + \text{Fe}_2\text{O}_3 + \text{Na}_2\text{O} + \text{K}_2\text{O} + \text{TiO}_2)] * 101.96$ ;  $S = [\text{mol. prop.} (\text{SiO}_2 - 2\text{Na}_2\text{O} - 2\text{K}_2\text{O})] * 60.09$ . Position of the four vertices of the tetrahedron:  $Q = S$ ,  $Ol = M_2S$ ,  $CaTs = CAS$ ,  $Di = CMS_2$ . Triangular inserts are zooms of the grey area at the Fo vertex of the tetrahedron and show a comparison between representative mass balanced results and natural "slightly enriched xenoliths" when increasing percentages of (a) a silica-poor, high Ca/(Mg, Fe) component (e.g., post Archean Terrains average; Rudnick and Fountain, 1995) is added to an undepleted mantle region (e.g., 25AMlh); (b) a silica-rich, low Ca/(Mg, Fe) component (e.g., 701 Ssand, pelagic sediment; Planck and Langmuir, 1998) is added to a fertile mantle region (e.g., 36Mlh). Insert (c) shows the variations of meaningful trace element ratios (normalized to the primordial mantle; McDonough and Sun, 1995; see Table 5b) produced by increasing percentages of the metasomatic agent as in (b), while a hypothetical trend representing the effect of a OIB-like component (e.g., VVP host rocks) in modifying the composition of the infiltrated xenoliths is reported in (d) for a qualitative comparison. Noteworthy, two "slightly enriched xenoliths" show major element compositions that suggest olivine enrichment during partial melting events, plotting toward the Fo vertex in the Fo-CaTs-Q-Di tetrahedron. Sp: spinel; ol: olivine; cpx: clinopyroxene; opx: orthopyroxene represent the compositions of the mineral phases adopted for these calculations.

the mineral phases ( $a_{i,j} = \text{constant}$ ), but changing their proportions by using a least-squared based mass balance calculation (e.g., Stomer and Nicholls, 1978). This provides an estimate of the weight fraction of the solid phases  $j$  of given compositions in the metasomatized assemblage ( $P_j^*$ ) that are necessary to obtain the starting bulk composition in order to get:

$$F_i = \sum a_{i,j} (P_j^*)$$

In Table 5, the major element compositions of the primary assemblages, metasomatic liquids and calculated products are compared to the observed metasomatized assemblages. Mass balanced weight modal compositions

of reactants and products are reported for control on mineral phases during the reaction (Table 5a). Significant results for incompatible trace element ratios and Sr isotopes are reported in Table 5b. The least-square residual is always lower than 0.5 and generally ~0.2–0.3. Our results highlight how the addition of silica-rich and/or silica-poor liquids to a variably fertile mantle region may cause significant olivine consumption and orthopyroxene growing in the secondary assemblage, while spinel percentage is only slightly affected by such metasomatic reactions. Clinopyroxene is preferentially melted if silica-rich, low Ca/(Mg, Fe) sediments are a significant component in the metasomatic liquid. It is important to note that the presence of pyrometamorphic textures indicates the clinopyroxene breakdown (see Table 1). On the other hand, the modal abundance of clinopyroxene grows if the metasomatic agent is characterized by the presence of silica-poor, high Ca/(Mg, Fe) sediments (Table 5a). Major and trace element compositions of the “slightly enriched xenoliths” can be obtained by the addition of about:

a) 2–8% of a silica-poor, high Ca/(Mg, Fe) metasomatic agent (e.g., from terrigenous sediments) to a not enriched, or slightly depleted, mantle source (e.g., 25AMlh or MA7), or

b) 2–5% of a silica-rich, low Ca/(Mg, Fe) metasomatic agent (e.g., from pelagic sediments) to an undepleted and unmetasomatized, or slightly fertile, mantle source (e.g., 36MLh or SG3).

As far as the above percentages, mass balance calculations on major and trace elements gave coherent results.

Our modeling is represented and summarized in Fig. 9, where variations in major element compositions, induced by addition of metasomatic liquids with a sedimentary signature to various hypothetical primary mantle assemblages, are projected onto the forsterite (Fo)-Ca-Tschermak (CaTs)-Quartz (Qz) plane of the Qz-Fo-CaTs-Di (diopside) system, after recast of analyses in terms of CMAS components (O’Hara, 1968). Such a representation allows a comprehensive overview of the whole major element characteristics of each natural and calculated compositions we investigated. Moreover, the effects induced by increasing percentages of one of the two metasomatic agents on the major and trace element compositions of a slightly fertile mantle source can be compared focusing on Figs. 9b and c.

On the basis of petrologic observation (e.g., clinopyroxene showing clear disequilibria textures and relatively high modal amounts of orthopyroxene), we argue that the slab-derived metasomatism of the VVP lithosphere was likely related to a silica-rich, Ca-poor agent, likely enriched in a pelagic sediment component. Compositions of the VVP xenoliths which show geochemical features similar to sedimentary material suggest that slab-derived enrichment processes might have

affected a relatively fertile mantle region beneath the SE Alps.

In summary, the VVP lithosphere was a variably depleted upper mantle that experienced a complex metasomatic process induced by both a slab-derived component, and OIB-like melts in a variable way. Metasomatism by dehydration and melting of a subducted plate, and interaction with OIB-like melts ( $^{87}\text{Sr}/^{86}\text{Sr} \leq 0.7033$ ,  $^{143}\text{Nd}/^{144}\text{Nd} \sim 0.5129$ ,  $^{206}\text{Pb}/^{204}\text{Pb} > 19.5$  ratios, and  $\delta^{18}\text{O} \sim 6\text{‰}$ ) may account for the present geochemical and isotopic heterogeneity of the VVP lithospheric mantle. The slab-derived component is easily traceable to the South-eastward subduction of the European plate underneath the African plate, which was a long-running phenomenon (140–40 Ma) responsible for the closure of the Alpine Tethys (Schmid *et al.*, 1997; Ranalli *et al.*, 2004). This process involved the sinking of the Ligurian-Piedmont and Valais oceans (probably rich in marine sediments) and the Briançonnais microcontinent (carrier of a terrigenous sediment signature), culminating with the collision of the Eurasian and Apulia plates (Dal Piaz and Venturelli, 1983; Stampfli *et al.*, 2001). Evidence for subduction-related metasomatism in the VVP lithospheric mantle comes from the high Ba/La, La/Nb, and U/Th ratios, with  $\delta^{18}\text{O} \sim 7\text{‰}$ , observed in several VVP xenoliths. These features are akin to those of altered oceanic crust and its pelagic sediment veneer (Elliott *et al.*, 1997). The geodynamic scenario proposed by Macera *et al.* (2003, 2004) and Ranalli *et al.* (2004) may explain the occurrence of both OIB-HIMU-type and subduction-related metasomatism in the VVP mantle lithosphere. According to this model, since the Cretaceous a mantle plume with OIB-HIMU geochemical signature was situated in the upper mantle, above the transition zone. Local favorable tectonic conditions, e.g., brief extensional phases or slab breakoff, might have caused upwelling of mantle plume material with subsequent partial melting episodes of the plume material. The flux of liquids released by partial melting of the plume might have induced the OIB-HIMU metasomatism in the overriding lithospheric mantle.

## SUMMARY AND CONCLUSIONS

In comparison to the primordial mantle, the VVP ultramafic xenoliths (mg# >88) are slightly to strongly depleted in a basaltic component. The presence of glass patches and strong iron enrichment coupled with a slight increase of the Cr/(Cr + Al) ratio in spinel, apparently not related to interaction with the host basalt, are likely due to reactions between the VVP xenoliths and different metasomatic agents, that occurred early in the history of the Veneto lithosphere. The nature of the metasomatic agents was constrained by comparing the geochemical and isotopic features of the VVP xenoliths, such as variable

Ba/LREE, LILE-LREE/HFSE and LREE/HREE ratios, discordant Nb, Ta, Sr and K anomalies, high  $^{207}\text{Pb}/^{204}\text{Pb}$  together with relatively low  $^{206}\text{Pb}/^{204}\text{Pb}$  ratios, and significantly high Sr and oxygen isotopic compositions. Mass balance calculations support that different metasomatic components affected the VVP subcontinental mantle:

a) an OIB-like agent related to upwelling of deep mantle material characterized by high Th/REE, Th/U, LREE/HREE, LILE/HREE ratios,  $^{87}\text{Sr}/^{86}\text{Sr} \leq 0.7033$ ,  $^{143}\text{Nd}/^{144}\text{Nd} \sim 0.5129$ ,  $^{206}\text{Pb}/^{204}\text{Pb} > 19.5$  ratios and  $\delta^{18}\text{O} \sim 6\text{‰}$ ;

b) silica-rich liquids, likely enriched in sedimentary material belonging to the European subducted slab. This upper crust-like component is characterized by high LFSE/HFSE, LREE/HFSE and variable Ba/LREE ratios,  $^{87}\text{Sr}/^{86}\text{Sr} \geq 0.7035$ ,  $^{143}\text{Nd}/^{144}\text{Nd} < 0.5130$ ,  $^{206}\text{Pb}/^{204}\text{Pb} \leq 19.5$  isotope composition, and average  $\delta^{18}\text{O} \geq 7\text{‰}$ .

The VVP peridotites reflect a subcontinental mantle source that has been affected by complex enrichment processes, related to a geodynamic scenario dominated by extension-related magmatism (Cenozoic sodic-alkaline volcanism), but neighboring active collision (subduction of the European slab).

**Acknowledgments**—K. Maffei (Pisa University) is thanked for her analytical work and help with sample collection. R. Carampin at C.N.R.-I.G.G. (Padova unit) is acknowledged for technical assistance during EPM analyses. Many thanks to B. Galland (Lab. Tectonophysique, Montpellier 2), P. Brunet (Paul Sabatier University, Toulouse), and P. T  louk (E.N.S. Lyon) for their technical assistance during isotope analyses, and to P. Armienti for helpful discussion. Our thanks go also to the reviewers, K. Ozawa and A. Beard, for constructive criticism of the manuscript. A review of an earlier version of the manuscript by H. Downes helped us to clarify our ideas and is greatly appreciated. The Universities of Bologna and Pisa are gratefully acknowledged. Financial support by Finanziamento MIUR 2001-2003, prot. n   2001048823 (Morten, L., Macera, P.: “Natura e composizione dei vari serbatoi coinvolti nella genesi del magmatismo Terziario Alpino: implicazioni geodinamiche”).

## REFERENCES

- Alibert, C., Michard, A. and Albar  de, F. (1983) The transition from alkali basalts to kimberlites: isotopes and trace element evidence from melilitites. *Contrib. Mineral. Petrol.* **82**, 176–186.
- Beccaluva, L., Bonadiman, C., Coltorti, M., Salvini, L. and Siena, F. (2001) Depletion events, nature of metasomatizing agent and timing of enrichment processes in lithospheric mantle xenoliths from the Veneto Volcanic Province. *J. Petrol.* **42**, 173–187.
- Bedini, R. M., Bodinier, J.-L., Dautria, J. M. and Morten, L. (1997) Evolution of LILE-enriched small melt fractions in the lithospheric mantle: a case study from the East African Rift. *Earth Planet. Sci. Lett.* **153**, 67–83.
- Ben Othman, D., White, W. M. and Patchett, J. (1989) The geochemistry of marine sediments, island arc magma genesis, and crust-mantle recycling. *Earth Planet. Sci. Lett.* **94**, 1–21.
- Bodinier, J.-L., Dupuy, C. and Dostal, J. (1988) Geochemistry and petrogenesis of eastern Pyrenean peridotites. *Geochim. Cosmochim. Acta* **52**, 2893–2907.
- Bodinier, J.-L., Vasseur, G., Verni  res, J., Dupuy, C. and Fabri  s, J. (1990) Mechanisms of mantle metasomatism: geochemical evidence from the Lherz orogenic peridotite. *J. Petrol.* **31**, 597–628.
- Bonadiman, C., Coltorti, M., Milani, L., Salvini, L., Siena, F. and Tassinari, R. (2001) Metasomatism in the lithospheric mantle and its relationships to magmatism in the Veneto Volcanic Province, Italy. *Per. Mineral.* **70**, 333–357.
- Carignan, J., Ludden, J. and Francus, S. (1996) On the recent enrichment of subcontinental lithosphere: a detailed U-Pb study of spinel lherzolite xenoliths, Yukon, Canada. *Geochim. Cosmochim. Acta* **60**, 4241–4252.
- Carpenter, R. L., Edgar, A. D. and Thibault, Y. (2002) Origin of spongy textures in clinopyroxene and spinel from mantle xenoliths, Hessian Depression, Germany. *Miner. Petrol.* **74**, 149–162.
- Chauvel, C., Hofmann, A. W. and Vidal, P. (1992) HIMU-EM: the French Polynesian connection. *Earth Planet. Sci. Lett.* **110**, 99–119.
- Chazot, G., Menzies, M. A. and Harte, B. (1996) Silicate glasses in spinel lherzolites from Yemen: origin and chemical compositions. *Chem. Geol.* **134**, 159–179.
- Chen, S., O’Reilly, S. Y., Zhou, X., Griffin, W. L., Zhang, G., Sun, M., Feng, J. and Zhang, M. (2001) Thermal and petrological structure of the lithosphere beneath Hannuoba, Sino-Korean Craton, China: evidence from xenoliths. *Lithos* **56**, 267–301.
- Chiba, H., Chacko, T., Clayton, R. N. and Goldsmith, J. R. (1989) Oxygen isotope fractionations involving diopside, forsterite, magnetite and calcite: application to geothermometry. *Geochim. Cosmochim. Acta* **53**, 2985–2995.
- Coltorti, M., Bonadiman, C., Hinton, R. W., Siena, F. and Upton, G. J. (1999) Carbonatite metasomatism of the oceanic upper mantle: evidence from clinopyroxenes and glasses in ultramafic xenoliths of Grande Comore, Indian Ocean. *J. Petrol.* **40**, 133–165.
- Coltorti, M., Beccaluva, L., Bonadiman, C., Salvini, L. and Siena, F. (2000) Glasses in mantle xenoliths as geochemical indicators of metasomatic agents. *Earth Planet. Sci. Lett.* **183**, 303–320.
- Dal Piaz, G. V. and Venturelli, G. (1983) Brevi riflessioni sul magmatismo post-ofiolitico nel quadro dell’evoluzione spazio-temporale delle Alpi. *Mem. Soc. Geol. It.* **26**, 5–19.
- Davis, A. C., Bickle, M. J. and Teagle, D. A. H. (2003) Imbalance in the oceanic strontium budget. *Earth Planet. Sci. Lett.* **211**, 173–187.
- De Francesco, A. M. and Morten, L. (1991) Glass bearing ultramafic xenoliths in basanites from Monti Lessini, Veneto region, Northern Italy: evidence of ultrapotassic melts in the upper mantle. *Plinius* **4**, 54–55.

- De Vecchi, G. and Sedeà, R. (1995) The Paleogene basalts of the Veneto Region (NE Italy). *Mem. Sci. Geol.* **47**, 253–274.
- Dérulle, B., Harmon, R. S. and Moorbath, S. (1983) Combined Sr-O isotope relationships and petrogenesis of Andean volcanics of South America. *Nature* **302**, 814–816.
- Downes, H. (2001) Formation and modification of the shallow sub-continental lithospheric mantle: a review of geochemical evidence from ultramafic xenolith suites and tectonically emplaced ultramafic massifs of western and central Europe. *J. Petrol.* **42**, 233–250.
- Downes, H. and Dupuy, C. (1987) Textural, isotopic and REE variations in spinel peridotite xenoliths, Massif Central, France. *Earth Planet. Sci. Lett.* **82**, 121–135.
- Downes, H., Embey-Isztin, A. and Thirlwall, M. F. (1992) Petrology and geochemistry of spinel peridotite xenoliths from the western Pannonian basin (Hungary): evidence for an association between enrichment and texture in the upper mantle. *Contrib. Mineral. Petrol.* **109**, 340–354.
- Downes, H., Kostoula, T., Jones, A. P., Beard, A. D., Thirlwall, M. F. and Bodinier, J.-L. (2002) Geochemistry and Sr-Nd isotopic compositions of mantle xenoliths from the Monte Vulture carbonatite-melilitite volcano, central southern Italy. *Contrib. Mineral. Petrol.* **144**, 78–92.
- Downes, H., Reichow, M. K., Mason, P. R. D., Beard, A. D. and Thirlwall, M. F. (2003) Mantle domains in the lithosphere beneath the French Massif Central: trace element and isotopic evidence from mantle clinopyroxenes. *Chem. Geol.* **200**, 71–87.
- Eiler, J. M., Crawford, A., Elliott, T., Farley, K. A., Valley, J. W. and Stolper, E. M. (2000) Oxygen isotope geochemistry of oceanic-arc lavas. *J. Petrol.* **41**, 229–256.
- Elliott, T., Plank, T., Zindler, A., White, W. and Bourdon, B. (1997) Element transport from slab to volcanic front at the Mariana arc. *J. Geophys. Res.* **102**, 14991–15019.
- Foden, J., Song, S. H., Turner, S., Elburg, M., Smith, P. B., Van der Steldt, B. and Van Penglis, D. (2002) Geochemical evolution of lithospheric mantle beneath SE South Australia. *Chem. Geol.* **182**, 663–695.
- Franz, L., Becker, K. P., Kramer, W. and Herzig, P. M. (2002) Metasomatic mantle xenoliths from the Bismarck microplate (Papua New Guinea)—thermal evolution, geochemistry and extent of slab-induced metasomatism. *J. Petrol.* **43**, 315–343.
- Franzini, M., Leoni, L. and Saitta, M. (1975) Revisione di una metodologia analitica per fluorescenza-X, basata sulla correzione completa degli effetti di matrice. *Rend. Soc. It. Mineral. Petrol.* **31**, 365–378.
- Garrison, J. R., Jr. and Taylor, L. A. (1981) Petrogenesis of pyroxene-oxide intergrowths from kimberlite and cumulate rocks: co-precipitation or exsolution? *Am. Mineral.* **66**, 723–740.
- Gill, J. B. (1981) *Orogenic Andesites and Plate Tectonics*. Springer-Verlag, Berlin, 101 pp.
- Grégoire, M., Lorand, J. P., Cottin, J. Y., Giret, A., Mattielli, N. and Weis, D. (1997) Xenoliths evidence for a refractory oceanic mantle percolated by basaltic melts beneath the Kerguelen archipelago. *Eur. J. Mineral.* **9**, 1085–1100.
- Green, T. H. and Adam, J. (2003) Experimentally-determined trace element characteristics of aqueous fluid from partially dehydrated mafic oceanic crust at 3.0 GPa, 650–700°C. *Eur. J. Mineral.* **15**, 815–830.
- Griffin, W. L., O'Reilly, S. and Stabel, A. (1988) Mantle metasomatism beneath western Victoria, Australia: II. Isotopic geochemistry of Cr-diopside lherzolites and Al-Augute pyroxenites. *Geochim. Cosmochim. Acta* **52**, 449–457.
- Harris, N. B. W., Pearce, J. A. and Tindle, A. G. (1986) Geochemical characteristics of collision-zone magmatism. *Collision Tectonics* (Coward, M. P. and Reis, A. C., eds.), 67–81, Geol. Soc. London, Spec. Publ., London 19.
- Hartmann, G. and Wedepohl, K. H. (1990) Metasomatically altered peridotite xenoliths from the Hessian Depression (Northwest Germany). *Geochim. Cosmochim. Acta* **54**, 71–86.
- Hauri, E. H., Shimizu, N., Dieu, J. J. and Hart, S. R. (1993) Evidence for hotspot-related carbonatite metasomatism in the oceanic upper mantle. *Nature* **365**, 221–227.
- Hawkesworth, C. K., Gallagher, K., Hergt, J. M. and McDermott, F. (1994) Destructive plate margin magmatism: geochemistry and melt generation. *Lithos* **33**, 169–188.
- Hegner, E., Satir, M. and Morten, L. (1990) Upper mantle composition beneath Northern Italy: isotopic evidence from alkali basalts and lherzolite nodules (abstract) International Volcanologic Congress, Mainz.
- Ikeda, Y., Nagao, K. and Kagami, H. (2001) Effects of recycled materials involved in a mantle source beneath the southwest Japan arc region: evidence from noble gas, Sr, and Nd isotopic systematics. *Chem. Geol.* **175**, 509–522.
- Ionov, D. A., Prikhod'ko, V. S. and O'Reilly, S. Y. (1995) Peridotite xenoliths in alkali basalts from the Sikhote-Alin, southeastern Siberia, Russia: trace-element signatures of mantle beneath a convergent continental margin. *Chem. Geol.* **120**, 275–294.
- Ito, E. and Stern, R. J. (1985) Oxygen and strontium isotopic investigations of subduction zone volcanism: the case of the volcano arc and Marianas island arc. *Earth Planet. Sci. Lett.* **76**, 312–320.
- Javoy, M. (1980)  $^{18}\text{O}/^{16}\text{O}$  and D/H ratios in high temperatures peridotites. *Orogenic Mafic Ultra-mafic Association* **272**, 279–287.
- Klemme, S., Van der Laan, S. R., Foley, S. F. and Gunther, D. (1995) Experimentally determined trace and minor element partitioning between clinopyroxene and carbonatite melt under upper mantle conditions. *Earth Planet. Sci. Lett.* **133**, 439–448.
- Kogiso, T., Tatsumi, Y. and Nakano, S. (1997) Trace element transport during dehydration processes in the subducted oceanic crust: 1. Experiments and implications for the origin of ocean island basalts. *Earth Planet. Sci. Lett.* **148**, 193–205.
- Kramm, U. and Wedepohl, K. H. (1990) Tertiary basalts and peridotite xenoliths from the Hessian Depression (NW Germany), reflecting mantle compositions low in radiogenic Nd and Sr. *Contrib. Mineral. Petrol.* **106**, 1–8.
- Lenoir, X., Garrido, C. J., Bodinier, J.-L. and Dautria, J. M. (2000) Contrasting lithospheric mantle domains beneath the Massif Central (France) revealed by geochemistry of peridotite xenoliths. *Earth Planet. Sci. Lett.* **181**, 359–375.

- Leoni, L. and Saitta, M. (1976) X-Ray fluorescence analysis of 29 trace elements in rock and mineral standards. *Rend. Soc. It. Mineral. Petrol.* **32**, 497–510.
- Macera, P., Gasperini, D., Piromallo, C., Blichert-Toft, J., Bosch, D., Del Moro, A. and Martin, S. (2003) Geodynamic implications of deep mantle in the source of Tertiary volcanics from the Veneto region (South-Eastern Alps). *J. Geodynamics* **36**, 563–590.
- Macera, P., Gasperini, D., Bosch, D., Faccenna, C., Piromallo, C., Ranalli, G. and Mahatsente R. (2004) HIMU-OIB magmatism in subduction zones: An example from the Italian south-eastern Alps (abstract). *Geochim. Cosmochim. Acta* **68**, A5.3.43.
- Maffei, K., Gasperini, D., Piromallo, C., Macera, P., Bosch, D., Faccenna, C., Martin, S. and Ranalli, G. (2003) Lower mantle upwelling in subduction zones: an example from the Italian South Eastern Alps (abstract). *Geophysical Research* **5**, EAE03-A-09705.
- Magaritz, M., Whitford, D. J. and James, D. E. (1978) Oxygen isotopes and the origin of high  $^{87}\text{Sr}/^{86}\text{Sr}$  andesites. *Earth Planet. Sci. Lett.* **40**, 220–230.
- Manhès, J., Minster, J. F. and Allègre, C. J. (1978) Comparative uranium-thorium-lead and rubidium-strontium study of the Saint Severine amphoterite: consequences for early solar system chronology. *Earth Planet. Sci. Lett.* **39**, 14–24.
- Mattey, D., Lowry, D. and Macpherson, C. (1994) Oxygen isotope composition of mantle peridotite. *Earth Planet. Sci. Lett.* **128**, 231–241.
- Mattielli, N., Weis, D., Grégoire, M., Mennessier, J. P., Cottin, J. Y. and Giret, A. (1996) Kerguelen basic and ultrabasic xenoliths: evidence for long-lived Kerguelen hotspot activity. *Lithos* **37**, 261–280.
- Maury, R. C., Defant, M. J. and Joron, J. L. (1992) Metasomatism of the sub-arc mantle inferred from trace elements in Philippine xenoliths. *Nature* **360**, 661–663.
- McDonough, W. F. (1990) Constraints on the composition of the continental lithospheric mantle. *Earth Planet. Sci. Lett.* **101**, 1–18.
- McDonough, W. F. and McCulloch, M. T. (1987) The southeast Australian lithospheric mantle: isotopic and geochemical constraints on its growth and evolution. *Earth Planet. Sci. Lett.* **86**, 327–340.
- McDonough, W. F. and Sun, S. S. (1995) Composition of the Earth. *Chem. Geol.* **120**, 223–253.
- Mercier, J. C. C. and Nicolas, A. (1975) Textures and fabrics of upper-mantle peridotites as illustrated by xenoliths from basalts. *J. Petrol.* **16**, 454–487.
- Milani, L., Beccaluva, L. and Coltorti, M. (1999) Petrogenesis and evolution of the Euganean magmatic complex, Veneto Region, North-East Italy. *Eur. J. Mineral.* **11**, 379–399.
- Morten, L. (1971) Noduli ultrafemici nel basalto di S. Giovanni Ilarione (Valle dell'Alpone, M. Lessini, Verona). *Mineral. Petrogr. Acta* **17**, 15–40.
- Morten, L. (1987) Italy: a review of xenolithic occurrences and their comparison with Alpine peridotites. *Mantle Xenoliths* (Nixon, P. H., ed.), 135–148, J. Wiley and Sons.
- Morten, L. and Bondi, M. (1981) Spinel lherzolite inclusions in basalts from Monti Lessini, Veneto Region, northern Italy. *N. Jb. Miner. Mh.* **7**, 308–316.
- Morten, L. and De Francesco, A. M. (1991) Glasses in mantle-derived xenoliths from the basanitic rocks of Monti Lessini, Veneto region, Northern Italy (abstract). *Plinius* **6**, 172–173.
- Morten, L., Taylor, L. A. and Durazzo, A. (1989) Spinel in harzburgite and lherzolite inclusions from the San Giovanni Ilarione Quarry, Lessini Mountains, Veneto region, Italy. *Mineral. Petrol.* **40**, 74–89.
- Morten, L., Zanetti, A., Vannucci, R. and Rizzo, G. (2002) Mantle metasomatism beneath the Veneto Volcanic Province (North Italy) as recorded by the geochemical signatures of clinopyroxene and glasses from xenoliths in Tertiary volcanics. *International Workshop on Orogenic Lherzolites and Mantle Processes* 4th, 104–105.
- Morten, L., Zanetti, A., Braga, R. and Vannucci, R. (2004) Trace element composition of clinopyroxenes and glasses from xenoliths in tertiary volcanics of the Veneto Volcanic Province (northern Italy): evidence for multistage evolution via partial melting and melt-mantle interaction (abstract). *Int. Geol. Congr.* 32nd, A255-23.
- Muehlenbachs, K. and Clayton, R. N. (1972) Oxygen isotopes studies of fresh and weathered submarine basalts. *Canadian J. Earth Sci.* **9**, 172–182.
- Nelson, D. R., Chivas, A. R., Chappell, B. W. and McCulloch, M. T. (1988) Geochemical and isotopic systematics in carbonatites and implications for the evolution of ocean-island sources. *Geochim. Cosmochim. Acta* **52**, 1–17.
- Neumann, E. R., Wulff-Pedersen, E., Pearson, N. J. and Spencer, E. A. (2002) Mantle xenoliths from Tenerife (Canary Islands): evidence for reactions between mantle peridotites and silicic carbonatite melts inducing Ca metasomatism. *J. Petrol.* **43**, 825–857.
- O'Hara, M. J. (1968) The bearing of phase equilibria studies in synthetic and natural systems on the origin and evolution of basic and ultrabasic rocks. *Earth. Sci. Rev.* **4**, 69–133.
- O'Reilly, S. and Griffin, W. L. (1988) Mantle metasomatism beneath western Victoria, Australia: I. Metasomatic processes in Cr-diopside lherzolites. *Geochim. Cosmochim. Acta* **52**, 433–447.
- Parkinson, I. J. and Pearce, J. A. (1998) Peridotites from the Izu-Bonin-Mariana forearc (ODP Leg 125): evidence for mantle melting and melt-mantle interaction in a supra-subduction zone setting. *J. Petrol.* **39**, 1577–1618.
- Peslier, A. H., Francis, D. and Ludden, J. (2002) The lithospheric mantle beneath continental margins: melting and melt-rock reaction in Canadian Cordillera xenoliths. *J. Petrol.* **43**, 2013–2047.
- Pike, N. J. E. and Schwarzman, E. C. (1977) Classification of textures in ultramafic xenoliths. *J. Geol.* **85**, 49–61.
- Pineau, F., Semet, P., Grassineau, N., Okrugin, V. M. and Javoy, M. (1999) The genesis of the stable isotope (O, H) record in arc magmas: the Kamtchatka's case. *Chem. Geol.* **153**, 93–124.
- Planck, T. and Langmuir, C. H. (1998) The chemical composition of subducting sediment and its consequences for the crust and mantle. *Chem. Geol.* **145**, 325–394.
- Qi, Q., Taylor, L. A. and Zhou, X. (1995) Petrology and geochemistry of mantle peridotite xenoliths from SE China. *J. Petrol.* **36**, 55–79.
- Ranalli, G., Gasperini, D., Macera, P. and Mahatsente, R. (2004)

- Subduction of continental lithosphere, changes in negative buoyancy, and slab-plume interaction: consequences for slab breakoff (abstract). *Geophys. Res.* **6**, EGU04-A-02044.
- Ringwood, A. E. (1975) *Composition and Petrology of the Earth's Mantle*. McGraw-Hill, New York.
- Rosenbaum, J. M., Wilson, M. and Downes, H. (1997) Multiple enrichment of the Carpathian-Pannonian mantle: Pb-Sr-Nd isotope and trace element constraints. *J. Geophys. Res.* **102**, 14947–14961.
- Rudnick, R. L. and Fountain, D. M. (1995) Nature and composition of the continental crust: a lower crustal perspective. *Rev. Geophys.* **33**, 267–309.
- Rudnick, R. L., McDonough, W. F. and Chappel, B. C. (1993) Carbonatite metasomatism in the northern Tanzanian. *Earth Planet. Sci. Lett.* **114**, 463–475.
- Schmid, S. M., Pfiffner, O. A., Schoenborn, G., Froitzheim, N. and Kissling, E. (1997) Integrated cross section and tectonic evolution of the Alps along the eastern traverse. *Results of NRP20; Deep Structure of the Swiss Alps* (Pfiffner, O. A., Lehner, P., Heitzman, P., Mueller, S. and Steck, A., eds.), 289–304.
- Siena, F. and Coltorti, M. (1989) Lithospheric mantle evolution: evidences from ultramafic xenoliths in the Lessinian volcanics (Northern Italy). *Chem. Geol.* **77**, 347–364.
- Song, Y. and Frey, F. A. (1989) Geochemistry of peridotite xenoliths in basalt from Hannuoba, Eastern China: implications for subcontinental mantle heterogeneity. *Geochim. Cosmochim. Acta* **53**, 97–113.
- Stampfli, G. M., Mosar, J., Favre, P., Pilleveit, A. and Vannay, J. C. (2001) Permo-Mesozoic evolution of the western Tethyan realm: the Neotethys/East-Mediterranean connection. *PeriTethys Memoir 6: Peritethyan Rift/Wrench Basins and Passive Margins*, IGCP 369 (Ziegler, P. A., Cavazza, W., Robertson, A. H. F. and Crasquin-Soleau, S., eds.), 51–108, Mém. Museum Nat. Hist. Nat. 186.
- Stormer, J. C. and Nicholls, J. (1978) XLFRAC: a program for the interactive testing of magmatic differentiation models. *Comput. Geosci.* **4**, 153–159.
- Stosch, H. G. and Lugmair, G. W. (1986) Trace element and Sr and Nd isotope geochemistry of peridotite xenoliths from the Eifel (West Germany) and their bearing on the evolution of the subcontinental lithosphere. *Earth Planet. Sci. Lett.* **80**, 281–298.
- Sun, S. S. and McDonough, W. F. (1989) Chemical and isotopic systematics of oceanic basalts: implications for mantle composition and processes. *Magmatism in the Ocean Basins* (Saunders, A. D. and Norry, M. J., eds.), 313–345, Geol. Soc. Spec. Publ. London 42.
- Takazawa, E., Frey, F. A., Shimizu, N., Obata, M. and Bodinier, J.-L. (1992) Geochemical evidence for melt migration and reaction in the upper mantle. *Nature* **359**, 55–58.
- Tatsumoto, M., Basu, A. R., Wankang, H., Junwen, W. and Guanghong, X. (1992) Sr, Nd, and Pb isotopes of ultramafic xenoliths in volcanic rocks of Eastern China: enriched components EMI and EMII in subcontinental lithosphere. *Earth Planet. Sci. Lett.* **113**, 107–128.
- Taylor, H. P. (1968) The oxygen isotope geochemistry of igneous rocks. *Contrib. Mineral. Petrol.* **19**, 1–71.
- Taylor, H. P. (1986) Igneous rocks II: isotopic case studies of circum Pacific magmatism. *Stables Isotopes in High Temperature. Geological Processes* (Valley, J. W., Taylor, H. P., Jr. and O'Neil, J. R., eds.), *Reviews in Mineralogy* (Ribes, P. H., ed.), 273–317, Am. Mineral. Soc.
- Taylor, H. P., Jr. and Sheppard, S. M. F. (1986) Igneous rocks: I. Processes of isotopic fractionation and isotope systematics. *Stables Isotopes in High Temperature. Geological Processes* (Valley, J. W., Taylor, H. P., Jr. and O'Neil, J. R., eds.), *Reviews in Mineralogy* (Ribes, P. H., ed.), 227–271 Am. Mineral. Soc.
- Taylor, H. P., Jr. and Turi, B. (1976) High-<sup>18</sup>O igneous rocks from the Tuscan Magmatic Province, Italy. *Contrib. Mineral. Petrol.* **55**, 33–54.
- Taylor, S. R. and McLennan, S. M. (1985) *The Continental Crust: Its Composition and Evolution. An Examination of the Geochemical Record Preserved in Sedimentary Rocks*. Blackwell Sc. Publ., Oxford.
- Taylor, W. R. (1998) An experimental test of some geothermometer and geobarometer formulations for upper mantle peridotites with application to the thermobarometry of fertile lherzolite and garnet websterite. *N. Jb. Miner. Abh.* **172**, 381–408.
- Vaselli, O., Downes, H., Thirlwall, M., Dobosi, G., Coradossi, N., Seghedi, I., Szakacs, A. and Vannucci, R. (1995) Ultramafic xenoliths in Plio-Pleistocene alkali basalts from the Eastern Transylvanian Basin: depleted mantle enriched by vein metasomatism. *J. Petrol.* **36**, 23–53.
- Vidal, P., Dupuy, C., Maury, R. and Richard, M. (1989) Mantle metasomatism above subduction zones: trace-element and radiogenic isotope characteristics of peridotite xenoliths from Batan Island (Philippines). *Geology* **17**, 1115–1118.
- von Blanckenburg, F. and Davies, J. H. (1995) Slab breakoff: a model for syncollisional magmatism and tectonics in the Alps. *Tectonics* **14**, 120–131.
- Weaver, B. L. (1991) The origin of ocean island basalt end-member compositions: trace element and isotopic constraints. *Earth Planet. Sci. Lett.* **104**, 381–397.
- Weis, D., Demaiffe, D., Cauet, S. and Javoy, M. (1987) Sr, Nd, O and H isotopic ratios in Ascension Island lavas and plutonic inclusions; cogenetic origin. *Earth Planet. Sci. Lett.* **82**, 255–268.
- Wells, P. R. A. (1977) Pyroxene thermometry in simple and complex systems. *Contrib. Mineral. Petrol.* **62**, 2, 129–139.
- White, W. M. and Dupré, B. (1986) Sediment subduction and magma genesis in the Lesser Antilles; isotopic and trace element constraints. *J. Geophys. Res.* **91**, 5927–5941.
- White, W. M., Albarède, F. and Télouk, P. (2000) High precision analysis of Pb isotopic ratios using multi-collector ICP-MS. *Chem. Geol.* **167**, 257–270.
- Whitehouse, M. J. and Neumann, E. R. (1995) Sr-Nd-Pb isotope data for ultramafic xenoliths from Hierro, Canary Islands: melt infiltration processes in the upper mantle. *Contrib. Mineral. Petrol.* **119**, 239–246.
- Wiechert, U., Ionov, D. A. and Wedepohl, K. H. (1997) Spinel peridotite xenoliths from the Atsagin-Dush volcano, Dariganga lava plateau, Mongolia: a record of partial melting and cryptic metasomatism in the upper mantle. *Contrib. Mineral. Petrol.* **126**, 345–364.
- Wilshire, H. G. and Shervais, J. W. (1975) Al-augite and Cr-

- diopside ultramafic xenoliths in basaltic rocks from Western U.S. *Phys. Chem. Earth*, **9**, 257–272.
- Witt-Eickchen, G. (1993) Upper mantle xenoliths from alkali basalts of the Vogelsberg, Germany: implications for mantle upwelling and metasomatism. *Eur. J. Mineral.* **5**, 361–376.
- Wood, D. A. (1980) The application of a Th-Hf-Ta diagram to problems of tectonomagmatic classification and to establishing the nature of crustal contamination of basaltic lavas of the British Tertiary Volcanic Province. *Earth Planet. Sci. Lett.* **50**, 11–30.
- Wulff-Pedersen, E., Neumann, E. R. and Jensen, B. B. (1996) The upper mantle under La Palma, Canary Islands: formation of Si-K-Na-rich melt and its importance as a metasomatic agent. *Contrib. Mineral. Petrol.* **125**, 113–139.
- Yaxley, G. M. and Kamenetsky, V. (1999) In situ origin for glass in mantle xenoliths from southeastern Australia: insights from trace element composition of glasses and metasomatic phases. *Earth Planet. Sci. Lett.* **172**, 97–109.
- Yaxley, G. M., Crawford, A. J. and Green, D. H. (1991) Evidence for carbonatite metasomatism in spinel peridotite xenoliths from western Victoria, Australia. *Earth Planet. Sci. Lett.* **107**, 305–317.
- Yaxley, G. M., Green, D. H. and Kamenetsky, V. (1998) Carbonatite metasomatism in the southeastern Australian lithosphere. *J. Petrol.* **39**, 1917–1930.
- Zampieri, D. (1995) Tertiary extension in the Southern Trento Platform, Southern Alps, Italy. *Tectonics* **14**, 645–657.
- Zangana, N. A., Downes, H., Thirlwall, M. F. and Hegner, E. (1997) Relationship between deformation, equilibration temperatures, REE and radiogenic isotopes in mantle xenoliths (Ray Pic, Massif Central, France): and example of plume-lithosphere interaction? *Contrib. Mineral. Petrol.* **127**, 187–203.
- Zangana, N. A., Downes, H., Thirlwall, M. F., Marriner, G. F. and Bea, F. (1999) Geochemical variation in peridotite xenoliths and their constituent clinopyroxenes from Ray Pic (French Massif Central): implications for the composition of the shallow lithospheric mantle. *Chem. Geol.* **153**, 11–35.
- Zheng, Y. F. (1993) Calculation of oxygen isotope fractionation in anhydrous silicate minerals. *Geochim. Cosmochim. Acta* **57**, 1079–1091.